DIRECTION OF ARRIVAL ESTIMATION IN SENSOR ARRAYS WITH FAULTY ELEMENTS

A THESIS SUBMITTED TO
THE GRADUATE SCHOOL OF NATURAL AND APPLIED SCIENCES
OF
MIDDLE EAST TECHNICAL UNIVERSITY

BY

TAYFUN KÜLBAY

IN PARTIAL FULFILLMENT OF THE REQUIREMENTS
FOR
THE DEGREE OF MASTER OF SCIENCE
IN
ELECTRICAL AND ELECTRONICS ENGINEERING

JANUARY 2020

Approval of the thesis:

DIRECTION OF ARRIVAL ESTIMATION IN SENSOR ARRAYS WITH FAULTY ELEMENTS

submitted by **TAYFUN KÜLBAY** in partial fulfillment of the requirements for the degree of **Master of Science in Electrical and Electronics Engineering Department, Middle East Technical University** by,

Prof. Dr. Halil Kalıpçılar
Dean, Graduate School of **Natural and Applied Sciences** _____

Prof. Dr. İlkay Ulusoy
Head of Department, **Electrical and Electronics Eng.** _____

Prof. Dr. Engin Tuncer
Supervisor, **Electrical and Electronics Eng., METU** _____

Examining Committee Members:

Prof. Dr. Kemal Leblebicioğlu
Electrical and Electronics Eng., METU _____

Prof. Dr. Engin Tuncer
Electrical and Electronics Eng., METU _____

Prof. Dr. Buyurman Baykal
Electrical and Electronics Eng., METU _____

Prof. Dr. Yakup Özkazanç
Electrical and Electronics Eng., Hacettepe University _____

Prof. Dr. Umut Örgüner
Electrical and Electronics Eng., METU _____

Date: 31.01.2020

I hereby declare that all information in this document has been obtained and presented in accordance with academic rules and ethical conduct. I also declare that, as required by these rules and conduct, I have fully cited and referenced all material and results that are not original to this work.

Name, Surname: Tayfun Külbay

Signature:

ABSTRACT

DIRECTION OF ARRIVAL ESTIMATION IN SENSOR ARRAYS WITH FAULTY ELEMENTS

Külbay, Tayfun
Master of Science, Electrical and Electronics Engineering
Supervisor: Prof. Dr. Engin Tuncer

January 2020, 82 pages

During the operational lifetime of a sensor array, certain sensors cease to operate properly. The identification of these sensors is an important problem. Furthermore, the operation of the array is continued even with the faulty sensors. Therefore, new techniques are required in order to ensure that the system estimation performance does not degrade significantly. In this thesis, two different fault types in a sensor array are considered. The first fault type is special to MEMS microphone arrays. MEMS microphones are usually constructed with pairwise sensors which share the common data channel in positive and negative cycles of a clock signal. When one of the MEMS microphones is faulty, same data is seen for both of the microphone channels and determining the faulty sensor becomes a major problem. A new technique is developed to determine the faulty microphone based on the use of a source with known direction-of-arrival (DOA). This approach can find the faulty sensor or sensors accurately in low SNR depending on the source position with respect to the array. In a second fault type, it is assumed that each sensor's fault is associated with a probability. In other words, a sensor is either on or off with a probability "p" at any time. This problem is investigated in the literature before and G-MUSIC algorithm is proposed for a consistent DOA estimation. In this thesis, the problem scenario is investigated and a

new approach is proposed to estimate the DOA with a faulty sensor array. It is shown that the performance of the proposed algorithm is better than G-MUSIC.

Keywords: DOA Estimation, missing data, faulty sensor, MEMS microphone

ÖZ

SENSÖR DİZİLERİNDE HATALI SENSÖRLER İLE İŞARET GELİŞ AÇISI KESTİRİMİ

Külbay, Tayfun
Yüksek Lisans, Elektrik ve Elektronik Mühendisliği
Tez Danışmanı: Prof. Dr. Engin Tuncer

Ocak 2020, 82 sayfa

Bir sensör dizisinin operasyon zamanı boyunca, belirli sensörleri düzgün çalışmama durumuna geçebilir. Bu arızalı sensörlerin tespiti önemli bir sorundur. Aynı zamanda, hatalı sensörler bulunmasına rağmen sensör dizisinin çalışması devam etmektedir. Bu nedenle, sistemlerin tespit yeteneklerinde önemli bir performans bozukluğu yaşanmamasının sağlanması için yeni teknikler gerekmektedir. Bu tezde, iki farklı arızalı sensör tipi değerlendirilmiştir. Bunlardan ilki MEMS (Mikro Elektro Mekanik Sistemler) mikrofonları özelindedir. MEMS mikrofon dizileri genellikle negatif ve pozitif saat sinyalleri ile aynı veri kanalına sahip ikili sensörler olarak üretilirler. MEMS mikrofonlarından bir adeti arızalanır ise, ikili sensörlerin veri kanalından her ikisi için de aynı veri gözlemlenir ve hatalı sensörün tespiti büyük bir sorun haline gelir. Bu hatalı mikrofonun tespiti için işaret geliş açısı bilinen bir kaynak kullanılarak yeni bir metot geliştirildi. Bu yöntem, kaynağın sensör dizisine göre yerleşimine bağlı olarak düşük sinyal gürültü oranlarında oldukça başarılı sonuçlar vermektedir. İkinci arızalı sensör tipinde ise, her bir sensörün arıza durumunun olasılıksal olduğu varsayılmıştır. Başka bir deyişle, sensör herhangi bir zamanda "p" olasılığı ile çalışmakta veya çalışmamaktadır. Bu problem daha önce literatürde incelenmiş ve G-MUSIC algoritması ile tutarlı bir işaret geliş açısı kestirimi yapılabildiği önerilmiştir. Bu tezde ise, belirtilen problem senaryosu incelenmiş ve arızalı sensörler ile yeni bir

işaret geliş açısı kestirim yaklaşımı önerilmiştir. Performans kriterleri yönünden, yeni metodun G-MUSIC metodundan daha iyi olduğu gösterilmiştir.

Anahtar Kelimeler: İşaret Geliş Açısı Kestirimi, hatalı sensör, arıza, MEMS mikrofon

To my beloved ones…

ACKNOWLEDGEMENTS

First and foremost, I would like to thank my supervisor Prof. Dr. T. Engin Tuncer for his guidance through each stage of the process.

I am very grateful to Aselsan Inc. for supporting my research. Also, I would like to thank my colleague Meriç Sarıışık for his helpful contributions.

Finally, I would like to thank my family for their support through my whole life.

TABLE OF CONTENTS

LIST OF TABLES

TABLES

LIST OF FIGURES

FIGURES

LIST OF ABBREVIATIONS

ABBREVIATIONS

AOA	Angle of Arrival
CRLB	Cramer Rao Lower Bound
DOA	Direction of Arrival
DF	Direction Finding
EW	Electronic Warfare
ESPRIT	Estimation of Signal Parameters via Rotation Invariance Techniques
ELINT	Electronic Intelligence
MEMS	Micro Electro Mechanical Systems
MUSIC	Multiple Signal Classification
NCA	Non-Uniform Circular Array
NLA	Non-Uniform Linear Array
PCB	Printed Circuit Board
PTD	Probability of True Detection
RLA	Random Linear Array
RMSE	Root Mean Square Error
SCM	Sample Covariance Matrix
SNR	Signal to Noise Ratio
UCA	Uniform Circular Array
ULA	Uniform Linear Arrays

CHAPTER 1

INTRODUCTION

1.1. Background

Direction of Arrival (DOA) or Direction Finding (DF) estimation can be denoted as determining the bearing angle from a radiating emitter. It has a wide range of usage in many different areas for moving or stationary radiated sources, such as radar, sonar, navigation, wireless communication, Electronic Warfare (EW) applications. As a result of popular usage, there is a large DOA literature about its various methods and applications. One of the most popular literature work is [1] in order to get familiar with DOA applications and various methods with their advantages and disadvantages. For more specific works, [2-4] can be related with EW and Electronic Intelligence (ELINT) applications. In additionally, in [5-6] new algorithms and performance analysis for wireless communication applications take place in the literature.

In order to estimate the DOA of an emitter, firstly there should be sensor arrays that receive the radiated signal from the emitter. Moreover, sensor array geometry is crucial for Direction Finding performance of the system. The Uniform Linear Array (ULA) with maximum element spacing being less than half wavelength is commonly used for DOA applications due to its simplicity and ambiguity resistance. The spacing between sensors are equal. However, for different type of applications, performance and platform criteria, other array geometry structures can be used such as NLA (Non-Uniform Linear Array), UCA (Uniform Circular Array) or NCA (Non-Uniform Circular Array). NLA geometry is similar with ULA without having equal element spacing. In UCA case, the sensors in the array are positioned with equal spacing around a circle. Moreover, when sensors are positioned around a circle without having equal element spacing, array structure is called NCA.

Since the main topic is to estimate the bearing angle of radiated sources, DOA based estimation algorithms take the major part. Direction finding methods can be divided into two categories, classical and subspace based techniques. Classical methods basically estimate the DOA by scanning a beam through space and measuring the largest amount of power among each direction. One of the most popular classical method is the interferometer method which is an algorithm that estimates the DOA by correlating the received signal with the calibration data of the antenna that taken before [7]. Although classical methods are effective for DOA estimation, they have some disadvantages such as, they may fail completely for multiple sources. This brings us to the subspace based methods, in other words super-resolution techniques. MUSIC (Multiple Signal Classification) [8-10] and ESPRIT (Estimation of Signal Parameters via Rotation Invariance Techniques) [11, 12] methods are the most popular subspace based methods and both of them are sub-optimum methods. However, the thesis work focuses on MUSIC algorithm, since ESPRIT is not applicable for missing data arrays. The algorithm specifications of MUSIC, types, usage, advantages and disadvantages are explained in the related chapters.

In practical applications, during the lifetime of the sensors, some of the array elements might stop to operate properly. This can be denoted as faulty sensor or missing data problem. Facing with faulty sensor problem can cause from many things in practical applications. Firstly, most of the sensors are not resistant enough for humidity, water, dust or other environmental causes. One of the other reasons is over-heating. Since the antenna elements are used in a variety of applications, they can be effected from other system subparts' heat radiations. Additionally, array elements can be faced with physical impacts. As a result of facing with faulty sensors, faulty sensor detection and DOA estimation problems arise in practical applications.

Cases of Faulty Sensors

There are several types of faulty sensors which are encountered in practical applications. Some examples of the types of faulty sensor cases can be summarized as follows.

- Type 1: Sensor either operated properly (ON), or does not operate at all (OFF). In this case, if the sensor does not operate, output signal is zero. When the sensor output channel is corrupted by noise, noise can be observed at the output which may disguise the faulty sensor.
- Type 2: Sensor either operated properly (ON), or does not operate at all (OFF). In the case of the sensor is not operating, output signal is different from the desired signal but correlated. When the sensor output channel is corrupted by noise, sum of the correlated signal and noise can be observed at the output which may disguise the faulty sensor.
- Type 3: Sensor either operated properly (ON), or does not operate at all (OFF). In this case, if the sensor does not operate, output signal is entirely different from the desired signal, uncorrelated. When the sensor output channel is corrupted by noise, sum of the uncorrelated signal with noise can be observed at the output which may disguise the faulty sensor.
- Type 4: Sensor either operated properly (ON), or does not operate at all (OFF). This type of faulty sensor is special for the Micro Electro Mechanical Systems (MEMS) microphones and investigated in the thesis work as the deterministic problem. MEMS microphones are produced as pairwise sensors and these sensors share a common data channel with positive and negative clock cycles. Due to the common data channel, in the case of one of the pairwise sensors is not operating, output signal is the same with the pairwise operating sensor output signal.
- Type 5: Each sensor's fault is associated with a probability. In other words, a sensor is either operating (ON) or not operating (OFF) with a probability "p" at any time. The signal output is matched with the desired signal while sensor

is operating properly. However, in the case of the sensor is not operating, output signal is zero. When the sensor output channel is corrupted by noise, noise can be observed at the output which leads to detecting faulty sensor problems. This type of faulty sensor is investigated in the thesis work as the random array problem.

Faulty sensor existence in the sensor array is investigated in the thesis work as in two ways such as deterministic and random array problems.

In deterministic problem, one or more sensors might stop to operate completely. This can be seen in every kind of sensor in practical applications. However, MEMS microphones have a special case. MEMS microphones have a wide range of usage in DOA applications for localization of sound sources [13-14] since they meet the performance and SWAP-C (size, weight, power and cost) requirements. Because of MEMS microphones are produced as pairwise sensors onto a Printed Circuit Board (PCB) [15], these sensors share the common data channel in positive and negative cycles of the clock signal. When one of the pairwise MEMS microphones is faulty, operating microphone data is seen for both of the pairwise microphone channels. Therefore determining the faulty sensor becomes a major problem.

Although in the deterministic model the faulty sensor is not operating completely, in random array problem each sensor operate with a probability which corresponds to the randomly missing data. Moreover, randomly missing data leads to DOA estimation performance degradation. There are several studies according to performance analysis and consistent DOA estimation for missing data in the literature [16-17]. However, existing studies are not related with improving the DOA performance with detecting the faulty sensors where our motivation lies.

1.2. Scope and Contributions of the Thesis

In the thesis work, the missing data according to not operating sensor problem is investigated in two approaches, deterministic and random array approaches. Therefore, we proposed two methods for two different problems.

In the deterministic case, the important aspect is that it can be faced in practical applications due to the production of MEMS microphones. MEMS microphones are produced as pairwise sensors which have common data channel with positive and negative clock cycles. Because of having a common data channel, if one of the pairwise sensor is not operating, two microphone signals became exact copies of each other. As a result, determination of the faulty sensor becomes a major problem. In order to solve the problem, utilization of DOA applications are considered. By using a known DOA source, the faulty sensor or sensors in the array can be detected even in low SNR (Signal to Noise Ratio) values. Moreover, usage of a known source leads us to improve the DOA performance of the sensor array by detecting the faulty sensors without a physical intervention. Furthermore, faulty sensor problem is observed during our involvement with digital MEMS microphones for the construction of a massive microphone array [18] and it is reported for the first time in the literature.

In the second problem, the random array approach, each sensor element is operating according to a probability which is unknown. Hence, we are dealing with a random array whose elements are working according to an unknown probability which corresponds to the randomly missing data. Moreover, randomly missing data leads to DOA estimation performance degradation [17]. According to improving DOA performance in random array, several studies presented in the literature. The idea behind these studies is, estimating DOA by using the whole sensor array information without detecting operating and not operating sensors. The difference of the proposed method in the thesis work is improving the DOA performance by detecting the faulty sensors and eliminate their data. The results are shown that, proposed method achieves

higher DOA performances compared to the related studies. Additionally, the random array problem is investigated by assuming each sensor has a different operating probability rather than assuming equal operating probability in related studies. One of the other important aspect of thesis work is that, both Spectral MUSIC and Root-MUSIC estimation methods are used as a hybrid algorithm in order to achieve less computational complexity and higher performances. Finally, the proposed method is applicable for both single and multiple source DOA estimation applications.

CHAPTER 2

DIRECTION FINDING TECHNIQUES

2.1. Signal Model

The signal model for the Uniform Linear Array (ULA) geometry is introduced in this chapter. By using the signal model, DOA parameters are extracted which are used in the estimation problem. Moreover, the presented signal model is taken as a reference for the DOA estimation methods.

While the signal model is defined, several assumptions are considered.

Assumptions:

- Far-field
- Narrowband
- Sensor and sources exist in the same plane
- Sources are point emitters
- Homogenous Propagation Medium
- Calibrated Array

2.1.1. Far-field

In the far-field assumption, the distance between the array elements and radiating sources are supposed to be greater than the Rayleigh distance. Although the Rayleigh distance is the far-field specification limit, 10 times greater than the limit is usually considered to be a safe distance for assuming far-field. The Rayleigh distance equation is represented in Eqn. 2.1.

$$distance > \frac{2D^2}{\lambda} \tag{2.1}$$

where D is the array aperture and λ denotes the signal wavelength. The signal wavelength contains carrier frequency and speed of the signal in the propagation medium where it is shown in Eqn. 2.2.

$$\lambda = \frac{c}{f_c} \tag{2.2}$$

where c represents the speed of the signal in the propagation medium and f_c is the carrier frequency.

As a result of far-field distance assumption, time delay of incoming signals to the sensors can be written as a function of direction of arrival parameters of the signal.

2.1.2. Narrowband

For narrowband assumption, Eqn. 2.3 should be satisfied.

$$B \; x \; T_{max} \ll 1 \tag{2.3}$$

B denotes the bandwidth of the signal in *Hertz* where T_{max} is the maximum time to travel across the array.

2.1.3. Homogenous Propagation Medium

Homogenous propagation medium assumption is important since change in the medium can affect the signal features. For example, sound waves have different specifications in the sea water rather than signal waves in a homogenous propagation medium. Moreover, the speed of light is changeable due to the propagation medium.

2.1.4. Calibrated Array

In this assumption, the calibrated array stands for the sensors can be assumed Linear-Time-Invariant systems and their locations are known.

Since the assumptions are explained, signal model parameters are introduced in the following. By consideration of Fig 2.1, number of array elements is M, ϕ is the azimuth angle on xy plane starting from positive x-axis in counter clockwise direction and θ is the elevation angle starting to measure from positive z-axis.

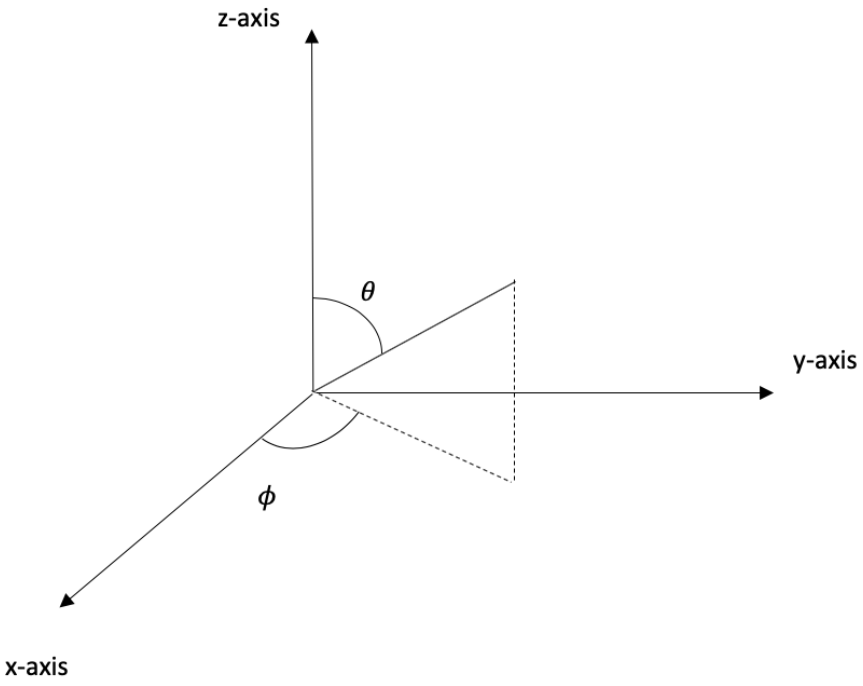

Figure 2.1. The Coordinate System

The received signal from M sensors can be written as,

$$s_{pi}(t) = s_p(t - \tau_i) = \Re\{s(t - \tau_i)e^{j2\pi f_c t}e^{-j2\pi f_c \tau_i}\}, i = 1, 2, \dots M \qquad (2.4)$$

where

$$s_p(t) \triangleq \Re\{s(t)e^{j2\pi f_c t}\} \qquad (2.5)$$

is the received signal from reference point.

$s(t)$ denotes the complex envelope for a specific sample t and τ_i is the time delay between the received signal taken from ith sensor and reference point. Notation of $\Re$ denotes the real term of the function. By using the narrowband assumption, the complex envelope can be written without the time delay in Eqn. 2.6.

$$s(t) \approx s(t-\tau) \tag{2.6}$$

Then by substituting Eqn. 2.6 into Eqn. 2.4, the received signal formulation can be rewritten as Eqn. 2.7.

$$s(t) = s_p(t-\tau_i) = \Re\{s(t)e^{j2\pi f_c t}e^{-j2\pi f_c \tau_i}\} \tag{2.7}$$

After demodulating and lowpass filtering, the baseband signal received from M sensors is given by,

$$y_i(t) = s(t)e^{-j2\pi f_c \tau_i} + \boldsymbol{n}(t), \qquad i = 1, 2, \ldots M \tag{2.8}$$

which $\boldsymbol{n}(t)$ refers as additive Gaussian noise.

Furthermore, the time delay of each sensor has (τ_i) in Eqn. 2.8 is written in Eqn. 2.9 as a function of coordinate angle parameters $\{\phi, \theta\}$ and Cartesian sensor positions (x, y, z) by using where it is mentioned in far-field assumption in Eqn. 2.9 which is valid when choosing the reference point as the center of the coordinate system (0, 0, 0).

$$\tau_i = \frac{1}{c}[x_i\cos(\theta)\sin(\phi) + y_i\sin(\theta)\sin(\phi) + z_i\cos(\theta)], i = 1, 2, \ldots M \tag{2.9}$$

$$\tau_i = \frac{\boldsymbol{g}^T\boldsymbol{p}_i}{c} \tag{2.10}$$

where

$$\boldsymbol{g} \triangleq [cos(\theta)sin(\phi)\ \ sin(\theta)sin(\phi)\ \ cos(\theta)]^T \tag{2.11}$$

$$\boldsymbol{p}_i \triangleq [x_i\ \ y_i\ \ z_i]^T \tag{2.12}$$

By substituting Eqn. 2.2 and 2.10 into Eqn. 2.8, the result is as

$$y_i(t) = s(t)e^{\frac{-j2\pi g^T P_i}{\lambda}} + n(t),\ \ i = 1, 2, \ldots M \tag{2.13}$$

From Eqn. 2.13, we can introduce array steering vector, $\boldsymbol{a}(\phi, \theta)$ in Eqn. 2.14, that contains all the spatial characteristics of array.

$$\boldsymbol{a}(\phi, \theta) \triangleq \begin{bmatrix} 1 \\ e^{\frac{-j2\pi g^T P_1}{\lambda}} \\ e^{\frac{-j2\pi g^T P_2}{\lambda}} \\ \vdots \\ e^{\frac{-j2\pi g^T P_{M-1}}{\lambda}} \end{bmatrix} \tag{2.14}$$

So, by substituting Eqn. 2.14 into Eqn. 2.13 we get Eqn. 2.15 as,

$$\boldsymbol{y}(t) = \boldsymbol{a}(\phi, \theta)s(t) + \boldsymbol{n}(t),\ \ t = 1, 2, \ldots N \tag{2.15}$$

N is the snapshot number where the waveform is sampled above the Nyquist rate. For direction of arrival estimation, these samples are used and analyzed.

Although, Eq. 2.14 is the single source case formulation, the model for multiple sources at directions $(\phi_1, \theta_1), \ldots\ (\phi_L, \theta_L)$ can be given as,

$$\boldsymbol{y}(t) = \boldsymbol{A}(\phi, \theta)\boldsymbol{s}(t) + \boldsymbol{n}(t),\ \ t = 1, 2, \ldots N \tag{2.16}$$

where

$$\boldsymbol{A}(\phi,\theta) \triangleq [\boldsymbol{a}(\phi_1,\theta_1)\ \boldsymbol{a}(\phi_2,\theta_2)\ \ldots\ \ldots\ \boldsymbol{a}(\phi_L,\theta_L)] \tag{2.17}$$

$\boldsymbol{A}(\phi,\theta)$ is the array steering matrix that contains all the steering vectors for the multiple sources. Furthermore, in Eqn. 2.18, the parameters in Eqn. 2.16 and Eqn. 2.15 are defined by showing their matrix sizes.

$$\begin{gathered}\boldsymbol{y}(t): received\ signal\ vector\ (Mx1)\\ \boldsymbol{A}(\phi,\theta): array\ steering\ matrix\ (MxL)\\ \boldsymbol{a}(\phi,\theta): array\ steering\ vector\ (Mx1)\\ \boldsymbol{s}(t): source\ signal\ vector\ (Lx1)\\ \boldsymbol{n}(t): additive\ Gaussian\ noise\ vector\ (Mx1)\\ M: number\ of\ sensors\ in\ the\ array\\ L: number\ of\ radiating\ sources\\ N: number\ of\ snapshots\end{gathered} \tag{2.18}$$

$$\boldsymbol{A}(\phi,\theta) = \begin{bmatrix} 1 & 1 & \cdots & 1 \\ e^{\frac{-j2\pi g_1^T P_{1,1}}{\lambda}} & e^{\frac{-j2\pi g_2^T P_{2,1}}{\lambda}} & \cdots & e^{\frac{-j2\pi g_L^T P_{L,1}}{\lambda}} \\ \vdots & \vdots & \vdots & \vdots \\ e^{\frac{-j2\pi g_1^T P_{1,M-1}}{\lambda}} & e^{\frac{-j2\pi g_2^T P_{2,M-1}}{\lambda}} & \cdots & e^{\frac{-j2\pi g_L^T P_{L,M-1}}{\lambda}} \end{bmatrix} \tag{2.19}$$

In Eqn. 2.19 array steering matrix is shown in detail where,

$$\boldsymbol{g}_l = [\cos(\theta_l)\sin(\phi_l)\ \ \sin(\theta_l)\sin(\phi_l)\ \ \cos(\theta_l)]^T \tag{2.20}$$

$$\boldsymbol{p}_{l,m} = \left[x_{l,m}\ \ y_{l,m}\ \ z_{l,m}\right]^T \tag{2.21}$$

ULA Case

By the definition of ULA, there are uniform, equally spacing between sensors in the array. Additionally, the sensors in the array are positioned only on one axis, otherwise the linearity specification could not be valid. The spacing between sensors are denoted as d. Consider $L = 1$ single source and M, number of sensors in the ULA geometry

with equal spacing between them. By arranging Eqn. 2.14, array steering vector is obtained for $\phi = \frac{\pi}{2}$.

$$\boldsymbol{a}(\theta) = \left[1 \;\; e^{\frac{-j2\pi}{\lambda}dsin(\theta)} \;\; \cdots \;\; e^{\frac{-j2\pi}{\lambda}(M-1)dsin(\theta)}\right]^T \tag{2.22}$$

In order to specify array steering vector in ULA uniquely, sensor phase difference should be equally less than π. By taking this into account, it is possible to compute the limits of the distance between the sensors in the array for an unambiguous array.

$$\frac{2\pi}{\lambda}dsin(\theta) \leq \pi \tag{2.23}$$

By eliminating π terms, and arranging the inequality we get,

$$dsin(\theta) \leq \frac{\lambda}{2} \tag{2.24}$$

Since the value range of sinus is $-1 \leq sin(x) \leq 1$, the distance between the sensors, d, should be chosen equally less than $\frac{\lambda}{2}$, in order to make the array steering vector unique for different angle of arrivals. This phenomena also corresponds for Shannon sampling theorem since,

$$f_s = \frac{f_c dsin(\theta)}{c} \Longrightarrow f_s \leq 0.5 \tag{2.25}$$

Unique array steering vector stands for an unambiguous array manifold. In other words, this is the condition for no spatial aliasing.

Eqn. 2.24 is derived for ULA geometry with M sensors and L number of sources. It should be noted that, the steering vector has Vandermonde structure which is special for ULA. ULA geometry has perfect solution for coherent signals due to its

Vandermonde structure. Moreover, forward-backward spatial smoothing can be applied for Vandermonde array structures [19].

As a result of deriving the array steering vector for ULA, the array steering matrix can be easily shown in Eqn. 2.26.

$$\boldsymbol{A}(\theta) = \begin{bmatrix} 1 & 1 & \cdots & 1 \\ e^{\frac{-j2\pi d\sin(\theta_1)}{\lambda}} & e^{\frac{-j2\pi d\sin(\theta_2)}{\lambda}} & \cdots & e^{\frac{-j2\pi d\sin(\theta_L)}{\lambda}} \\ \vdots & \vdots & \vdots & \vdots \\ e^{\frac{-j2\pi d(M-1)\sin(\theta_1)}{\lambda}} & e^{\frac{-j2\pi (M-1)d\sin(\theta_2)}{\lambda}} & \cdots & e^{\frac{-j2\pi (M-1)d\sin(\theta_L)}{\lambda}} \end{bmatrix} \quad (2.26)$$

2.2. Direction-Finding Algorithms

2.2.1. General Information

In this chapter, direction finding algorithms which are used in the thesis work are presented. Since DOA estimation has a wide usage in many areas, many different types of methods are derived. However, subspace-based methods are the most popular among them because of their robustness and low complexity. They are also referred as super resolution techniques. Top two subspace-base methods for DOA estimation are Multiple Signal Classification (MUSIC) [8-10] and Estimating Signal Parameter via Rotational Invariance Techniques (ESPRIT) [11, 12]. However, ESPRIT method is vulnerable for faulty sensor problems since it operates on a doublet structure, in other words it decomposes the sensor array into two sub-arrays. Therefore, MUSIC method is considered for faulty sensor problems.

Subspace-based methods for DOA estimation basically have two partitions of the observed data such as noise and signal subspaces. By solving the optimization problem over the projection of the observed data onto signal or noise subspace, the estimation of DOAs can be done.

2.2.2. MUSIC Algorithm

Multiple Signal Classification method is one of the most powerful methods in DOA estimation. There can be found many MUSIC-type estimation methods in the literature according to the desired goal for DOA estimation. Among these, two versions of MUSIC are frequently used in the thesis work. One of them is Spectral MUSIC and the other one is Root-MUSIC [20-21].

2.2.2.1. Spectral MUSIC

Spectral MUSIC is the most popular type of the MUSIC method family in DOA estimation. Spectral MUSIC algorithm uses the noise subspace and by projecting the observed data on the noise subspace, DOA estimations can be done. Basically it is a search algorithm, by searching all the angles in what range or resolution desired. As a result of being a search algorithm, MUSIC is not a fast algorithm, moreover computationally intense. However, its advantages make look the search algorithm disadvantages insignificant. Performance of DOA estimation, which is critical for an estimator, reaches the CRLB (Cramer Rao Lower Bound) [22] in ideal conditions. Ideal conditions stand for reaching infinite SNR value. Furthermore, one of the top advantages, Spectral MUSIC technique can be applied to any sensor geometry, without limits. Finally, Spectral MUSIC is a sub-optimum DOA estimation technique. So, in the following the DOA estimation based on Spectral MUSIC steps are presented.

DOA Estimation based on Spectral MUSIC

By remembering the signal model for ULA from previous chapter with M sensors and multiple sources, as L is the number of sources.

$$\boldsymbol{y}(t) = \boldsymbol{A}(\theta)\boldsymbol{s}(t) + \boldsymbol{n}(t) \ , \ \ t = 1, 2, \dots N \tag{2.27}$$

where N is the snapshot number. The array steering matrix is defined as Eqn. 2.28.

$$\boldsymbol{A}(\theta) = [\boldsymbol{a}(\theta_1)\ \boldsymbol{a}(\theta_2)\ \boldsymbol{a}(\theta_3)\ \ldots\ \ \boldsymbol{a}(\theta_L)] \tag{2.28}$$

By taking the covariance matrix of the received signal data $y(t)$ in Eqn. 2.27

$$\boldsymbol{R}_y = E[\boldsymbol{y}(t)\boldsymbol{y}^H(t)] = \boldsymbol{A}(\theta)\boldsymbol{s}(t)\boldsymbol{s}^H(t)\boldsymbol{A}^H(\theta) + \boldsymbol{n}(t)\boldsymbol{n}^H(t) \tag{2.29}$$

$$\boldsymbol{R}_s = E[\boldsymbol{s}(t)\boldsymbol{s}^H(t)] = \sigma_s^2\boldsymbol{I}\ ,\ \ E[\boldsymbol{n}(t)\boldsymbol{n}^H(t)] = \ \sigma_n^2\boldsymbol{I} \tag{2.30}$$

In Eqn. 2.30, signal and noise powers are defined. By using these two powers, SNR can be computed as in Eqn. 2.31.

$$SNR = \frac{\sigma_s^2}{\sigma_n^2} \tag{2.31}$$

By substituting Equations 2.29 and 2.30 we can rewrite the covariance matrix of the received signal as in Eqn. 2.32.

$$\boldsymbol{R}_y = \boldsymbol{A}(\theta)\boldsymbol{R}_s\boldsymbol{A}^H(\theta) + \sigma_n^2\boldsymbol{I} \tag{2.32}$$

After obtaining the covariance matrix of the observed data, it is divided into two partitions in order to obtain noise and signal subspace parameters. This division is known as eigen decomposition of the covariance matrix which is shown in Eqn. 2.33 and 2.34.

$$\boldsymbol{R}_y\boldsymbol{G} = \boldsymbol{G}\boldsymbol{\lambda} \tag{2.33}$$

$$\boldsymbol{R}_y \begin{bmatrix} \boldsymbol{g}_1 \\ \boldsymbol{g}_2 \\ \vdots \\ \boldsymbol{g}_M \end{bmatrix}^T = \begin{bmatrix} \boldsymbol{g}_1 \\ \boldsymbol{g}_2 \\ \vdots \\ \boldsymbol{g}_M \end{bmatrix}^T \begin{bmatrix} \lambda_1 & 0 & 0 & & & \\ 0 & \ddots & 0 & & 0 & \\ 0 & 0 & \lambda_L & & & \\ & & & 0 & 0 & 0 \\ & 0 & & 0 & \ddots & 0 \\ & & & 0 & 0 & 0 \end{bmatrix} \tag{2.34}$$

$$\boldsymbol{v} = [\boldsymbol{g}_1 \ \boldsymbol{g}_2 \ \dots \boldsymbol{g}_M]^T \tag{2.35}$$

$$\boldsymbol{\lambda} = diag\{\lambda_1, \lambda_2, \dots, \lambda_M\} \tag{2.36}$$

Above equations are valid for noise-free cases. In the presence of noise effect, noise contribution to the eigenvalues can be easily seen from Eqn. 2.37 by comparing with the noise-free case in Eqn. 2.34. Furthermore, the eigenvalues are added with noise variance σ_n^2.

$$\boldsymbol{\lambda} = \begin{bmatrix} \lambda_1 + \sigma_n^2 & 0 & 0 & & & \\ 0 & \ddots & 0 & & 0 & \\ 0 & 0 & \lambda_L + \sigma_n^2 & & & \\ & & & \sigma_n^2 & 0 & 0 \\ & 0 & & 0 & \sigma_n^2 & 0 \\ & & & 0 & 0 & \sigma_n^2 \end{bmatrix} \tag{2.37}$$

The eigenvalues can be sorted in descending way as, $\lambda_1 \geq \lambda_2 \geq \cdots \geq \lambda_L \geq \lambda_{L+1} \geq \cdots \geq \lambda_M$. Moreover, eigenvectors are sorted for corresponding eigenvalues as Eqn. 2.35.

Number of L eigenvalues, $\lambda_1 \geq \lambda_2 \geq \cdots \geq \lambda_L$, represent the eigenvalues of signal subspace. On the other hand, number of $M - L$ eigenvalues, $\lambda_{L+1} \geq \cdots \geq \lambda_M$, represent the eigenvalues of noise subspace. It can also be seen from Eqn. 2.37 that noise subspace eigenvalues are consisted of only noise variances. Similar with eigenvalues, number of L eigenvectors, $\boldsymbol{g}_1, \boldsymbol{g}_2, \dots, \boldsymbol{g}_L$, represent the eigenvectors of signal subspace, number of $M - L$ eigenvectors denote the noise subspace eigenvectors.

By taking the noise subspace eigenvectors in Eqn. 2.38 and array steering matrix,

$$\boldsymbol{G} = [\boldsymbol{g}_1, \boldsymbol{g}_2, \dots, \boldsymbol{g}_{M-L}] \tag{2.38}$$

MUSIC spectrum is obtained as in Eqn. 2.39.

$$p_{music}(\theta) = \frac{1}{\boldsymbol{A}^H(\theta)\boldsymbol{G}\boldsymbol{G}^H\boldsymbol{A}(\theta)} \tag{2.39}$$

Estimation of DOA's can be achieved by searching through the angles that maximizes the cost function in Eqn. 2.39.

$$\hat{\theta} = \underset{\theta}{\text{argmax}} \frac{1}{\boldsymbol{A}^H(\theta)\boldsymbol{G}\boldsymbol{G}^H\boldsymbol{A}(\theta)} \tag{2.40}$$

In order to avoid ambiguities, search angles should be chosen in the range of $[-\frac{\pi}{2}, \frac{\pi}{2}]$. Moreover, the search angle range is found by taking into account the behavior of $\sin(\theta)$ in the array steering matrix.

Spectral MUSIC in practical applications

- Compute the Sample Covariance Matrix (SCM)

$$\widehat{\boldsymbol{R}} = \frac{1}{N}\sum_{t=1}^{N} \boldsymbol{y}(t)\boldsymbol{y}^H(t) \tag{2.41}$$

- Find the noise subspace eigenvectors by using the eigen decomposition of SCM

$$\widehat{\boldsymbol{G}} = [\widehat{\boldsymbol{g}}_1, \widehat{\boldsymbol{g}}_2, \dots, \widehat{\boldsymbol{g}}_{M-L}] \tag{2.42}$$

- Solve the optimization problem by searching required angles in θ, estimate DOA

$$\hat{\theta} = \underset{\theta\in[-\frac{\pi}{2},\frac{\pi}{2}]}{\text{argmax}} \frac{1}{\boldsymbol{A}^H(\theta)\widehat{\boldsymbol{G}}\widehat{\boldsymbol{G}}^H\boldsymbol{A}(\theta)} \tag{2.43}$$

2.2.2.2. Root-MUSIC

Root-MUSIC is another class of MUSIC. Contrary of the Spectral MUSIC, Root-MUSIC is not a search estimation method, so it is a fast and computationally basic method comparing with Spectral MUSIC. Performance comparison between the

Spectral-MUSIC and Root-MUSIC is similar, both of them reach the CRLB in ideal conditions. However, it is stated that Root-MUSIC is superior to the Spectral MUSIC estimation [23]. Moreover, Root-MUSIC is a sub-optimum DOA estimation method. Unfortunately, Root-MUSIC can be applied only for linear array geometries such as ULA & NLA. In this part, the estimation methods of Root-MUSIC for both ULA & NLA are presented.

DOA Estimation based on Root-MUSIC for ULA

Consider the received signal for ULA geometry with M sensors and L number of sources as in Eqn. 2.44.

$$\boldsymbol{y}(t) = \boldsymbol{A}(\theta)\boldsymbol{s}(t) + \boldsymbol{n}(t) \ , \ t = 1, 2, \dots N \tag{2.44}$$

The covariance matrix of the observed signal and its eigen decomposition steps are the same with the Spectrum MUSIC method. So, we have the same eigenvectors of the noise subspace and array steering matrix with Spectrum MUSIC.

In Eqn. 2.45, the array steering vector for ith source is shown.

$$\boldsymbol{a}(\theta_i) = \left[1 \ e^{\frac{-j2\pi}{\lambda}dsin(\theta_i)} \ \dots \ e^{\frac{-j2\pi}{\lambda}(M-1)dsin(\theta_i)}\right]^T \tag{2.45}$$

The array steering vector is defined as including z-parameter in Eqn. 2.46.

$$\boldsymbol{a}(z) \triangleq \left[1 \ z^{-1} \ z^{-2} \ \dots \ z^{-(M-1)}\right]^T \tag{2.46}$$

where

$$z = e^{\frac{j2\pi}{\lambda}dsin(\theta)} \tag{2.47}$$

By using the orthogonality of the noise subspace eigenvectors to array steering vector, a polynomial equation for Root-MUSIC is obtained in Eqn. 2.48. This is similar with the MUSIC Spectrum, beside of z-parameters.

$$\boldsymbol{a}^T(z^{-1})\boldsymbol{G}\boldsymbol{G}^H\boldsymbol{a}(z) = 0, \qquad for\ L < M \tag{2.48}$$

Eqn. 2.48 is only valid when the number of sources, L, is less than number of sensors, M. In noise-free case, the roots of the Eqn. 2.48 lie on the unit circle. However, the roots of the polynomial equation does not lie on the unit circle because of the noise contribution. Furthermore, we pick the L nearest roots to the unit circle where they are inside the unit circle as well. By taking Eqn. 2.47 into consideration, DOA of L sources can be estimated from the picked L roots.

$$\varphi_{\hat{z}_i} = \frac{2\pi d}{\lambda}\sin(\theta_i) \tag{2.49}$$

$$\hat{\theta}_i = \sin^{-1}\left(\frac{\varphi_{\hat{z}_i}}{2\pi d}\lambda\right) \tag{2.50}$$

<u>Root-MUSIC for ULA in practical applications</u>

- Compute the SCM

$$\widehat{\boldsymbol{R}} = \frac{1}{N}\sum_{t=1}^{N}\boldsymbol{y}(t)\boldsymbol{y}^H(t) \tag{2.51}$$

- Find the noise subspace eigenvectors

$$\widehat{\boldsymbol{G}} = [\widehat{\boldsymbol{g}}_1, \widehat{\boldsymbol{g}}_2, \dots, \widehat{\boldsymbol{g}}_{M-L}] \tag{2.52}$$

- Find the roots, $\hat{z}_i$, of the spectrum polynomial

$$\boldsymbol{a}^T(z^{-1})\widehat{\boldsymbol{G}}\widehat{\boldsymbol{G}}^H\boldsymbol{a}(z) = 0 \tag{2.53}$$

- Estimate the DOAs from the L(number of sources) nearest roots to the unit circle where they are inside the unit circle as well.

$$\hat{\theta}_i = \sin^{-1}\left(\frac{\varphi_{\hat{z}_i}}{2\pi d}\lambda\right) \tag{2.54}$$

In order to avoid ambiguities, the roots can be eliminated to the first and the second quadrant of the Cartesian coordinate plane. In other words, the angle of estimated z-parameter should be chosen in the range of $\varphi_{\hat{z}_i} \in [-\frac{\pi}{2}, \frac{\pi}{2}]$.

DOA Estimation based on Root-MUSIC for NLA

Different from ULA, Non-Uniform-Linear-Array geometry does not have equal spacings between the sensor elements in the array. Therefore, the array steering matrix model differs in NLA case. Furthermore, according to [21], demonstrating Root-MUSIC with NLA results with better performance than ULA sensor array with using equal number of sensors.

Consider ULA geometry with some missing sensors in Fig 2.2.

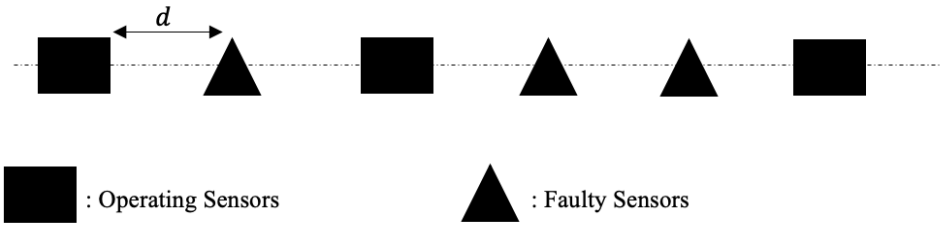

Figure 2.2. Non-Uniform Linear Array Structure

The array steering vector for ith source according to NLA geometry can be written as in Eqn. 2.55.

$$\boldsymbol{a}_{NLA}(\theta_i) = \left[e^{\frac{-j2\pi}{\lambda}c_1 d\sin(\theta_i)} \;\; e^{\frac{-j2\pi}{\lambda}c_2 d\sin(\theta_i)} \;\; \ldots \;\; e^{\frac{-j2\pi}{\lambda}c_M d\sin(\theta_i)}\right]^T \tag{2.55}$$

$$\boldsymbol{c} = [c_1, c_2, \dots, c_M] \tag{2.56}$$

c_m from Eqn.2.56 is the integer values in terms of distance d for existing sensors. Consider $\boldsymbol{c}$ vector for M=6 case as,

$$\boldsymbol{c} = [0 \;\; 2 \;\; 5] \tag{2.57}$$

The array steering vector of ith source is given as,

$$\boldsymbol{a}_{NLA}(\theta_i) = \left[1 \;\; e^{\frac{-j4\pi}{\lambda}dsin(\theta_i)} \;\; e^{\frac{-j10\pi}{\lambda}dsin(\theta_i)}\right]^T \tag{2.58}$$

Because of NLA is constructed by eliminating some sensors in the ULA geometry, the sensor number M is not valid for the array geometry. Number of sensors of NLA geometry has been denoted as M' which $M' \leq M$. The same orthogonality principle with Root-MUSIC for ULA is valid for Root-MUSIC for NLA, except the $\boldsymbol{a}(z)$ term.

$$\boldsymbol{a}_{NLA}^T(z^{-1})\boldsymbol{G}\boldsymbol{G}^H\boldsymbol{a}_{NLA}(z) = \; 0, \; L < M' \tag{2.59}$$

$$\boldsymbol{a}_{NLA}(z) = [z^{-c_1} \;\; z^{-c_2} \;\; z^{-c_3} \;\; \dots \;\; z^{-c_{M'}}]^T \tag{2.60}$$

Similar with the ULA case, roots of the polynomial do not lie on the unit circle because of the noise effect. By picking the L nearest roots to the unit circle where they are inside the unit circle, DOA of L sources can be estimated. Estimating DOAs from the chosen roots steps are the same with the Root-MUSIC ULA case.

$$\varphi_{\hat{z}_i} = \frac{2\pi d}{\lambda}\sin(\hat{\theta}_i) \tag{2.61}$$

$$\hat{\theta}_i = \sin^{-1}\left(\frac{\varphi_{\hat{z}_i}\lambda}{2\pi d}\right) \tag{2.62}$$

Root-MUSIC for NLA in practical applications

- Compute the SCM

$$\widehat{\boldsymbol{R}} = \sum_{t=1}^{N} \boldsymbol{y}(t)\boldsymbol{y}^{H}(t) \tag{2.63}$$

- Find the noise subspace eigenvectors

$$\widehat{\boldsymbol{G}} = [\widehat{\boldsymbol{g}}_1, \widehat{\boldsymbol{g}}_2, \dots, \widehat{\boldsymbol{g}}_{M-L}] \tag{2.64}$$

- Get the polynomial and find the roots of it $\hat{z}_i$

$$\boldsymbol{a}^{T}(z^{-1})\widehat{\boldsymbol{G}}\widehat{\boldsymbol{G}}^{H}\boldsymbol{a}(z) = 0 \tag{2.65}$$

- Estimate the DOAs from the L nearest roots to the unit circle where they are inside the unit circle as well.

$$\hat{\theta}_i = \sin^{-1}\left(\frac{ang(\hat{z}_i)}{2\pi d}\lambda\right) \tag{2.66}$$

Similar with the ULA case, in order to avoid ambiguities, the roots can be eliminated to the first and the second quadrant of the Cartesian coordinate plane. In other words, the angle of estimated z-parameter should be chosen in the range of $ang(\hat{z}_i) \in [-\frac{\pi}{2}, \frac{\pi}{2}]$.

2.2.2.3. G-MUSIC Algorithm

G-MUSIC is a form of weighted MUSIC estimation method that uses a different optimization problem than Spectral MUSIC, Eqn. 2.39. G-MUSIC method has been recently suggested as a result of investigation of finite snapshot situations that can be done better in the general asymptotic regime [24]. The asymptotic regime stands for where $M, N \to \infty, \frac{M}{N} = c$ where c is a constant greater than zero ($M > N$). Similar with the previous chapters, M is the number of sensors in the array and N is the number of snapshots. Moreover, according to a statistical comparison between G-

MUSIC and MUSIC [25], in case of closely spaced DOAs, G-MUSIC could consistently separate however MUSIC fails. The motivation for using G-MUSIC method is that, MUSIC-based DOA estimator appears to be inconsistent in the general asymptotic regime [26], although G-MUSIC based DOA estimates stated to be consistent in the general asymptotic regime for random array sensor probabilities $p \in (0,1)$ [27]. Consistent DOA estimations for random array statement is directly related with the problem investigated in the thesis work. Therefore, G-MUSIC DOA-based estimation method is utilized in the random array problem simulations in order to compare the performance of the proposed algorithm.

DOA Estimation based on G-MUSIC

As it is stated before, G-MUSIC solves different optimization problem rather than Spectral MUSIC's. However, the steps for the MUSIC and G-MUSIC before the minimization (optimization) step are the same. After sorting the eigenvalues in descending way Eqn. 2.67 is obtained as,

$$\lambda_1 \geq \lambda_2 \geq \cdots \lambda_L \geq \lambda_{L+1} \geq \cdots \geq \lambda_M \tag{2.67}$$

M is the number of sensors in the array and L is the source number. The eigenvectors corresponding to $\lambda_1 \geq \lambda_2 \geq \cdots \lambda_L$ are represented as signal subspace eigenvectors $\boldsymbol{S} = [\boldsymbol{s}_1, \boldsymbol{s}_2, \ldots \boldsymbol{s}_L]$ and corresponding to $\lambda_{L+1} \geq \cdots \geq \lambda_M$ eigenvalues are denoted as noise subspace eigenvectors $\boldsymbol{G} = [\boldsymbol{g}_1, \boldsymbol{g}_2, \ldots \boldsymbol{g}_{M-L}]$. Then, μ and v terms are obtained as the functions of sample eigenvalues in Eqn.2.68 and 2.69.

$$\mu(s) = \sum_{m=L}^{M-1} \frac{\lambda_{m+1}}{\lambda_s - \lambda_{m+1}} - \frac{k_{m+1}}{\lambda_s - k_{m+1}} \tag{2.68}$$

$$v(m) = \sum_{i=1}^{L} \frac{\lambda_i}{\lambda_{m+1} - \lambda_i} - \frac{k_i}{\lambda_{m+1} - k_i} \tag{2.69}$$

where $k_1 \geq k_2 \geq \cdots \geq k_M$ are the real valued solution of Eqn. 2.70. The real valued solutions of Eqn. 2.70 are sorted in descending order.

$$\sum_{m=1}^{M} \frac{\lambda_m}{\lambda_m - \boldsymbol{k}} = \frac{M}{c} = N \tag{2.70}$$

where $c = \frac{M}{N}$.

In Eqn. 2.71, G-MUSIC cost function is given by using μ and v weighting terms.

$$p_{gmusic}(\theta) = \boldsymbol{A}^H(\theta)\left(\sum_{s=1}^{L}(1+\mu(s))\boldsymbol{s}_s\boldsymbol{s}_s^* - \sum_{m=L}^{M-1} v(m)\boldsymbol{g}_{m-L+1}\boldsymbol{g}_{m-L+1}^*\right)\boldsymbol{A}(\theta) \tag{2.71}$$

Estimation of DOA's can be achieved by taking the θ angles that maximizes the G-MUSIC spectrum $p_{gmusic}(\theta)$.

$$\hat{\theta} = \underset{\theta \in \left[-\frac{\pi}{2},\frac{\pi}{2}\right]}{\operatorname{argmax}} p_{gmusic}(\theta) \tag{2.72}$$

G-MUSIC in practical applications

- Compute the Sample Covariance Matrix

$$\widehat{\boldsymbol{R}} = \sum_{t=1}^{N} \boldsymbol{y}(t)\boldsymbol{y}^H(t) \tag{2.73}$$

- Find the noise and signal subspace eigenvectors

$$\widehat{\boldsymbol{S}} = [\hat{\boldsymbol{s}}_1, \hat{\boldsymbol{s}}_2, \ldots \hat{\boldsymbol{s}}_L] \tag{2.74}$$

$$\widehat{\boldsymbol{G}} = [\hat{\boldsymbol{g}}_1, \hat{\boldsymbol{g}}_2, \ldots \hat{\boldsymbol{g}}_{M-L}] \tag{2.75}$$

- Compute the μ and v terms

$$\hat{\mu}(s) = \sum_{m=L}^{M-1} \frac{\hat{\lambda}_{m+1}}{\hat{\lambda}_s - \hat{\lambda}_{m+1}} - \frac{\hat{k}_{m+1}}{\hat{\lambda}_1 - \hat{k}_{m+1}} \tag{2.76}$$

$$\hat{v}(m) = \frac{\hat{\lambda}_1}{\hat{\lambda}_{m+1} - \hat{\lambda}_1} - \frac{\hat{k}_1}{\hat{\lambda}_{m+1} - \hat{k}_1} \tag{2.77}$$

- Solve the optimization problem by searching required angles in θ

$$\hat{\theta} = \underset{\theta \in \left[-\frac{\pi}{2}, \frac{\pi}{2}\right]}{\operatorname{argmax}} p_{gmusic}(\theta) \tag{2.78}$$

CHAPTER 3

DETERMINISTIC APPROACH FOR FAULTY SENSOR DETECTION

3.1. Problem Definition

In this chapter, the deterministic approach for faulty sensor problem is introduced. Moreover, the proposed detection of faulty sensor method is explained in detail. Then, the performance results of the proposed method are presented.

Detecting faulty sensors during operation of a sensor array is important since there are cases where the sensor malfunction due to several reasons. In addition, faulty sensor existence in the sensor array leads to DOA performance degradation. In the thesis work, Micro Electro Mechanical Systems (MEMS) microphones are assumed as faulty sensors and special case of them are examined.

Faulty Sensor Problem in MEMS Microphones

Micro Electro Mechanical Systems opened up new opportunities for microphone array construction and use. Especially digital MEMS microphones have several advantages compared to electret condenser microphones. They meet the SWAP-C (size, weight, power and cost) requirements in several applications. In fact, they have been recently used to construct massive microphone arrays which enable us to generate sharp beamformers for the isolation of closely spaced sound sources. Hence, MEMS microphones are used for DOA estimation applications [13-14].

One of the problems of digital MEMS microphone array production is the current feeding for the clock and data channels. When the number of microphones is large, the amount of current required to drive the clock and data channels increases. Furthermore the number of data buffer elements, which are used to latch the data and clock signals in order to transfer them distances exceeding 10 cm increases. One approach to alleviate this problem is to produce the MEMS microphones in doublets

on Printed Circuit Board (PCB) which share the same clock and data channels. Typical stereo MEMS microphone circuit can be seen in Fig 3.1. In this case, microphone data share the data channel at the positive and negative cycles of the common clock signal [15]. In this respect, each microphone should take the data channel at its own cycle. In other words, the microphones are configured to separate their output signal by using different edge of the clock signal, positive and negative cycles of clock. If one of the microphones is faulty, it cannot take the data channel and the data latched by the other microphone is still available for read. Hence, when the microphone channels are read, two microphone signals became exact copies of each other.

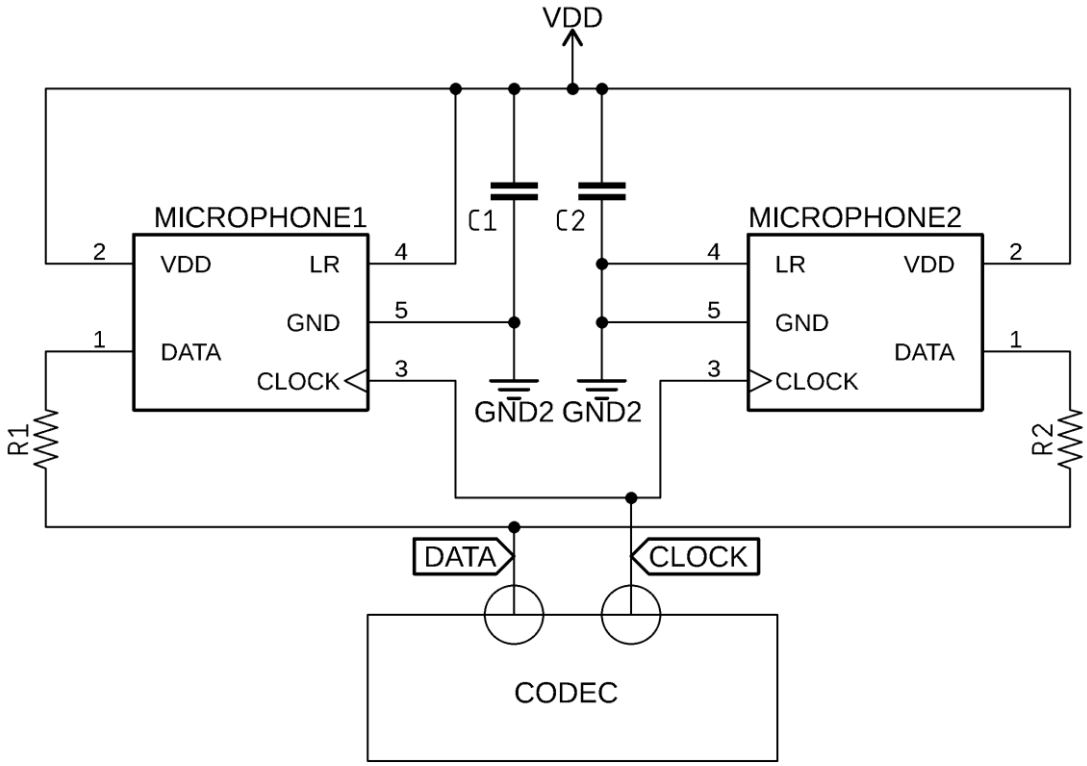

Figure 3.1. Typical digital MEMS Microphone application circuit

Although producing pairwise MEMS microphones are advantageous, this leads detection of faulty sensors in the array problem.

In Fig 3.2, the timing diagram of the MEMS microphone is shown where output channel reads the microphone data by using the positive or negative cycle of the clock signal.

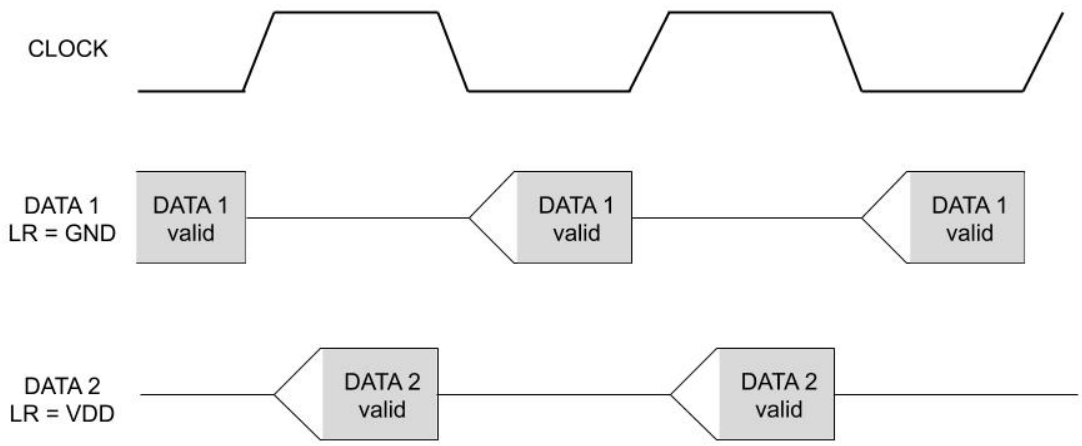

Figure 3.2. Timing Diagram of MEMS microphone

Faulty sensor detection can be done physically, through measuring the data channels of pairwise MEMS microphones with the help of an oscilloscope. In order to implement this task, the array elements should be uninstalled, preventing the operation of the sensor array. However, the desired goal is to determine the faulty sensors without a physical intervention to the sensor array and continue to operate. Hence, our motivation is to detect the faulty sensors by using a known DOA source during operation of the sensor array.

3.2. Problem Solution

In order to detect the faulty and operating sensors, DOA-based approach is investigated without solving the problem by uninstalling the sensors. This can be achieved by using a known DOA angle source.

In previous chapters, the signal model is presented when there is no faulty sensor in the array. When there are faulty sensors in the sensor array, signal model has to be modified. Consider one sensor is faulty and not operating in ULA structure like in Fig 3.3. Number of sensors in the array is, M =4, and assuming one of the first pairwise sensors is faulty. The known source direction angle is denoted as θ.

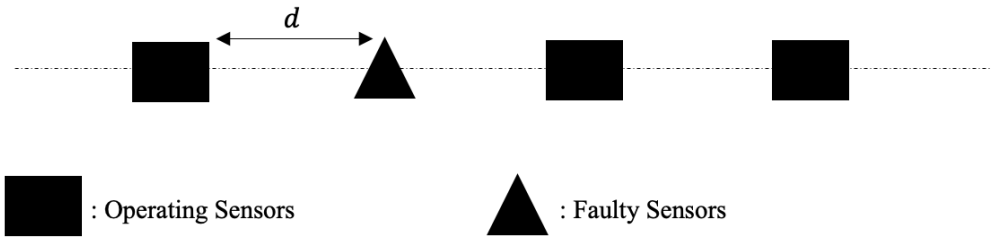

Figure 3.3. M=4 Sensor Array with Faulty Sensor

The distance between the sensors are chosen as $d = \frac{\lambda}{2}$, maximum element spacing without facing ambiguities. For modeling the faulty sensors, *operating sensor vector* is defined as in Eqn. 3.1 and 3.2.

$$c_i = \begin{cases} 1, & operating\ sensor \\ 0, & not\ operating\ sensor \end{cases} \tag{3.1}$$

$$\boldsymbol{c} = [c_1 \ \ c_2 \ldots \ \ c_M]^T \tag{3.2}$$

In Eqn. 3.1 and 3.2, c_i is an integer that corresponds to the number of the operating elements. $\boldsymbol{c}$ vector is the *operating sensor vector*. Operating sensor vector denotes which sensor is operating or not. Note that, $\boldsymbol{c}$ vector is the vector of true outcomes. In order to eliminate faulty sensors from the array steering vector, $\boldsymbol{T}$ matrix is defined. $\boldsymbol{T}$ matrix is obtained by taking the diagonal matrix of c_i, $diag\{c_i\}$, and then removing the ith rows corresponding to the faulty sensors in the array. $\boldsymbol{T}$ matrix is used remove the channel corresponding to the faulty sensors in the array. This is required in order have an appropriate array output and covariance matrix as in Eqn. 3.3.

$$\tilde{\boldsymbol{a}}(\theta) = \boldsymbol{T}\boldsymbol{a}(\theta) \tag{3.3}$$

An example of $\boldsymbol{c}$ and $\boldsymbol{T}$ matrices according to Fig 3.3 are shown in Eqn. 3.4 and 3.5.

$$\boldsymbol{c} = [1 \;\; 0 \;\; 1 \;\; 1]^T \tag{3.4}$$

$$\boldsymbol{T} = \begin{bmatrix} 1 & 0 & 0 & 0 \\ 0 & 0 & 1 & 0 \\ 0 & 0 & 0 & 1 \end{bmatrix} \tag{3.5}$$

$$\boldsymbol{a}(\theta) = \begin{bmatrix} 1 & e^{\frac{-j2\pi}{\lambda}dsin(\theta)} & e^{\frac{-j4\pi}{\lambda}dsin(\theta)} & e^{\frac{-j6\pi}{\lambda}dsin(\theta)} \end{bmatrix}^T \tag{3.6}$$

$$\tilde{\boldsymbol{a}}(\theta) = \begin{bmatrix} 1 & e^{\frac{-j4\pi}{\lambda}dsin(\theta)} & e^{\frac{-j6\pi}{\lambda}dsin(\theta)} \end{bmatrix}^T \tag{3.7}$$

As a result of the true array steering vector in Eqn. 3.7, the number of array sensors are decreased. So, operating number of sensors is denoted as M' where $M' \leq M$. M is the number of sensors in the array.

When the true array steering vector, $\tilde{\boldsymbol{a}}(\theta)$, is substituted in the array output, $\boldsymbol{y}(t)$, the true array output is obtained as,

$$\tilde{\boldsymbol{y}}(t) = \tilde{\boldsymbol{a}}(\theta)\boldsymbol{s}(t) + \boldsymbol{n}(t)\,, \qquad t = 1, 2, \ldots N \tag{3.8}$$

However, the true operating sensor vector, $\boldsymbol{c}$, is unknown in real life applications. Since it is assumed that only one sensor of the pairwise MEMS microphones is faulty, same sensor signal s observed for both of the sensor outputs. This generates a case where it is required to find which of the microphones is faulty. This problem can be resolved by considering all the possible cases of faulty sensors. Hence, we generate the possible operating sensor vectors, $\tilde{\boldsymbol{c}}$.

Consider the true operating sensor vector as $\boldsymbol{c} = [1\ \ 0\ \ 1\ \ 1]^T$ from Eqn. 3.4. Since it is known that the faulty sensor exist in the first pairwise sensors, the possible operating sensor vectors are as,

$$\tilde{\boldsymbol{c}}_{\boldsymbol{1}} = [1\ \ 0\ \ 1\ \ 1]^T \tag{3.9}$$
$$\tilde{\boldsymbol{c}}_{\boldsymbol{2}} = [0\ \ 1\ \ 1\ \ 1]^T \tag{3.10}$$

Possible array steering vectors, $\tilde{\boldsymbol{a}}_i(\theta)$, are obtained by using the possible operating sensors vectors and the corresponding $\tilde{\boldsymbol{T}}_{\boldsymbol{i}}$ matrix as in Eqn. 3.3.

$$\tilde{\boldsymbol{a}}_1(\theta) = \tilde{\boldsymbol{T}}_1\boldsymbol{a}(\theta) \tag{3.11}$$
$$\tilde{\boldsymbol{a}}_2(\theta) = \tilde{\boldsymbol{T}}_2\boldsymbol{a}(\theta) \tag{3.12}$$

Beside of the example in Fig 3.3, more than one sensor can be faulty. This brings in more possible $\tilde{\boldsymbol{c}}_i$, $\tilde{\boldsymbol{T}}_i$ and $\tilde{\boldsymbol{a}}_i$ vectors and matrices. Possibility number can be expressed as, 2^k. k is the number of faulty sensors.

In order to find the true configuration of the sensor array and the faulty sensors, DOA estimations, $\hat{\theta}_i$, are found for each possible array steering vectors by using the known DOA of the source and Spectral MUSIC algorithm. DOA estimations are obtained for each possible array steering vector, $\tilde{a}_i$, as in Eqn. 3.14 by searching through the angles that minimizes the MUSIC cost function given below,

$$p_{music,i}(\theta) = \frac{1}{\tilde{\boldsymbol{a}}_i^H(\theta)\boldsymbol{G}\boldsymbol{G}^H\tilde{\boldsymbol{a}}_i(\theta)} \tag{3.13}$$

$$\hat{\theta}_i = \underset{\theta}{\operatorname{argmax}}\, p_{music,i}(\theta) \tag{3.14}$$

Since the direction angle of the source is known, DOA performances can be computed from DOA estimations for each case. Therefore, the probability of true detection (PTD) of each sensor array configuration, $\tilde{\boldsymbol{c}}_i$, can be obtained for all trials which defines the confidence values of the possible array configurations according to the known source angles. PTD values are found by comparing the DOA absolute errors of possible configurations in Eqn. 3.15, where the minimum absolute error among the possible configurations considered as the true detection.

$$E_i = |\hat{\theta}_i - \theta| \tag{3.15}$$

As a result of computing the PTD's for each possible configurations where the true detection corresponds to the minimum absolute error, the best matching possible array configuration, $\hat{\boldsymbol{c}}$, is determined by picking the maximum PTD value. Furthermore, it is expected that the best matching possible array configuration corresponds to the true operating sensor vector, $\boldsymbol{c}$ vector. This leads to the detection of faulty sensors corresponding to the zero values in the $\hat{\boldsymbol{c}}$ by using DOA-based estimation.

The important aspect of the deterministic approach is determining the best angular region of the known source according to the sensor array. Because of the linear array structure and the faulty sensor, the DOA performance will not be the same in every source angle. In order to find the best angular region of the source angle, the features of ULA structure should be considered. Although element spacing is taken as $d = \lambda/2$ for ULA structure, the array structure with faulty elements has no longer the specifications of ULA. Therefore, the array structure is no longer has the ability of uniqueness for different angle of arrivals. In other words, instead of the right

configuration, the wrong possibility configurations may find the known source DOA correctly.

The angular sectors for the best faulty sensor detection can be identified by considering the correlations between the true array steering matrix with itself and the false array steering matrix. This leads us to the correlation graphs of array steering vectors for the search angles of MUSIC spectrum.

Define,

$$\boldsymbol{\beta}(\theta_1, \theta_2) \triangleq \frac{|\boldsymbol{a}^H(\theta_1)\boldsymbol{a}(\theta_2)|}{M} \tag{3.16}$$

where θ_1 is the true angle for the true array steering vector and θ_2 is the search angle for the correlated array steering vector.

Let $M = 6$ and $\tilde{\boldsymbol{a}}_1$ denotes the true array steering vector and $\tilde{\boldsymbol{a}}_2$ is the false possible array steering vector, corresponding to $\tilde{\boldsymbol{c}}_1 = [1\ 1\ 0\ 1\ 1\ 1]^T$ and other wrong possible operating sensor vector $\tilde{\boldsymbol{c}}_2 = [1\ 1\ 1\ 0\ 1\ 1]^T$ with one faulty sensor in the array. Correlations are obtained as in Eqn. 3.17 and 3.18 and the multi-dimensional plots of these correlations are presented in Fig. 3.4 and 3.5.

$$\boldsymbol{\beta}_{true}(\theta_1, \theta_2) = \frac{|\tilde{\boldsymbol{a}}^H{}_1(\theta_1)\tilde{\boldsymbol{a}}_1(\theta_2)|}{M-1} \tag{3.17}$$

$$\boldsymbol{\beta}_{false}(\theta_1, \theta_2) = \frac{|\tilde{\boldsymbol{a}}^H{}_1(\theta_1)\tilde{\boldsymbol{a}}_2(\theta_2)|}{M-1} \tag{3.18}$$

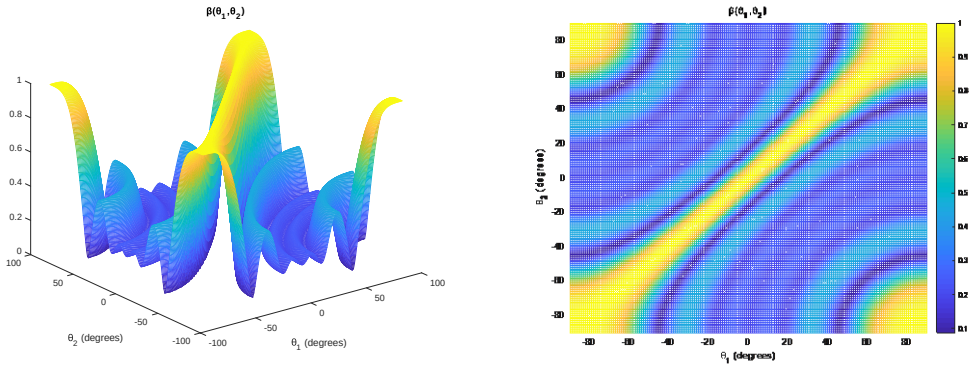

Figure 3.4. Correlation of True Array Steering Vector

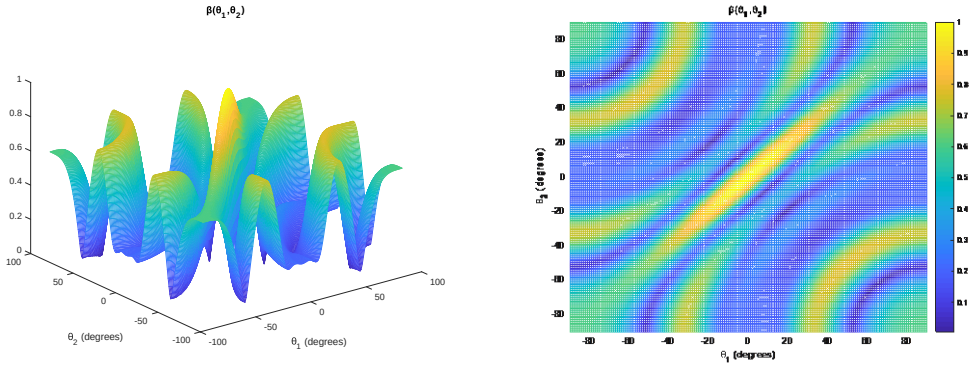

Figure 3.5. Correlation between True and False Array Steering Vectors

In Fig 3.4 it is observed that the correlation of the true array steering vector matches with the scanned steering vector at those points where the search angle is close to the true angle at the diagonal terms of the two dimensional graphs. In addition, true array steering vector does not match exactly with the scanned steering vector at the diagonal -90 and 90 degrees where DOA performance is poor at this angular region. Moreover, at the boresight of the array (0 degrees), matching search angles region corresponds to exactly with the correct angles where DOA performance is best. In addition, there are no ambiguities since no largely separated angles in $\boldsymbol{\beta}_{true}(\theta_1, \theta_2)$ graph. However, in Fig 3.5, as expected, the diagonal terms of the correlation between the true and false array steering vectors results nearly the same characteristics at the diagonal between -20 and 20 degrees. As a result, at the boresight of the antenna array, all possible array configurations operate good enough to find the true DOAs where it is not

recommended to position the known source in these angles according to the array structure, especially in low SNR cases. Also, ambiguities might be faced by using the wrong array steering vector. Therefore, the best angular region for faulty sensor detection can be found corresponding to the highest values in Fig. 3.4 which is at the same time corresponding to the lowest values in Fig. 3.5. This problem can be casted as maximizing the following cost function, namely,

$$\max_{\theta_2} \boldsymbol{\beta}_{true}(\theta_1, \theta_2) + (1 - \boldsymbol{\beta}_{false}(\theta_1, \theta_2)) \tag{3.19}$$

Above problem does not require an optimization procedure and can be solved by considering all the possible cases easily. $\boldsymbol{\beta}_{true}(\theta_1, \theta_2)$ and $\boldsymbol{\beta}_{false}(\theta_1, \theta_2)$ are normalized to one and Fig. 3.6 shows the cost function in (3.19) for a single faulty sensor. The highest values in Fig. 3.6 correspond to the angles where the detection of faulty sensor can be made with the highest probability. If only the diagonal of this figure is considered, Figure 3.7 is obtained.

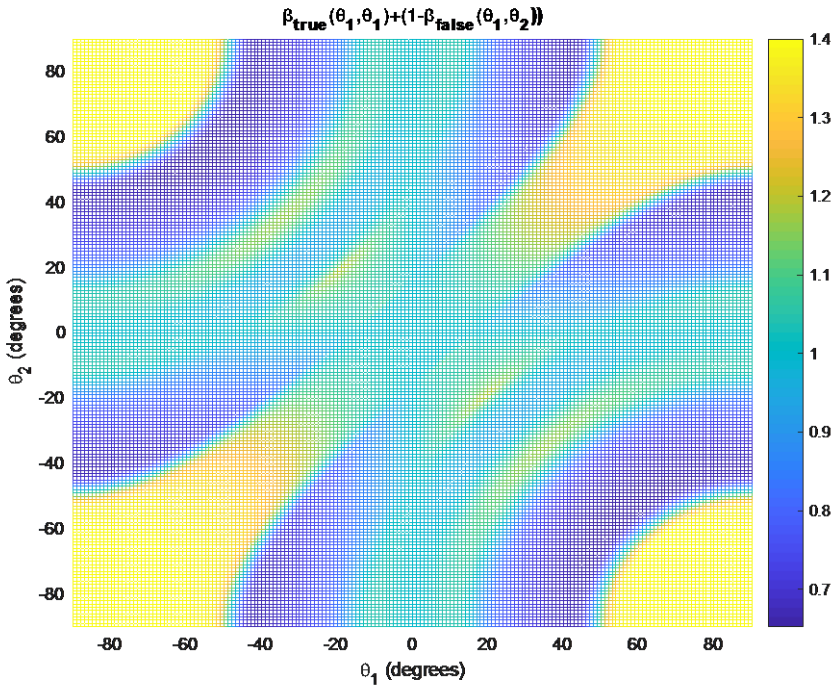

Figure 3.6. Correlation Cost Function

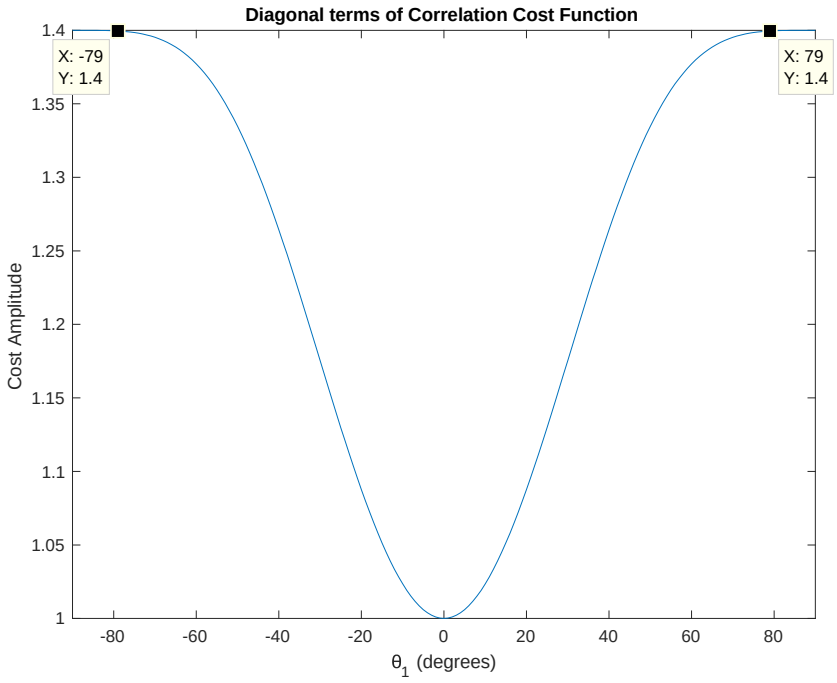

Figure 3.7. Diagonal terms of Correlation Cost Function

As it is shown in Fig. 3.7, the best source DOA angle is between -79 degrees and -90 degrees as well as their positive values. Since ULA resolution performance decreases towards the end-fire, the best source DOA angle in case of a single faulty sensor is ±79 degrees for ULA under ideal conditions. In other words, SNR is assumed to be sufficiently high. If SNR is decreased, then the effect of array resolution becomes a factor and the best angle is shifted towards broadside.

CHAPTER 4

RESULTS OF DETERMINISTIC METHOD FOR FAULTY DETECTION

In this part of thesis work, several simulations are done to show the performance of the proposed method as well as the dependence on the source DOA angle. Different scenarios are implemented including different SNR values, configurations of the faulty sensors and sensor element numbers. In all scenarios the array structures are assumed to be ULA and maximum element spacing $d = \frac{\lambda}{2}$. The DOA angle of the source is assumed to be known. Furthermore, the known source is rotated around the array in one degree resolution given in Fig. 4.1. At each emission point, array output is received by the array elements and then processed by the proposed approach to obtain the PTD curves. As a result, the response of the proposed approach for different source DOAs are evaluated. The noise vector $\boldsymbol{n}(t)$ is assumed as an additive Gaussian white noise with zero mean $E[\boldsymbol{n}(t)] = 0$. Moreover, noise and signal are assumed to be uncorrelated. The simulations are demonstrated in Matlab environment by performing 1000 Monte Carlo trials at each scenario.

The simulation results are divided into two parts as Scenario 1 and 2. In Scenario 1, only one faulty sensor exists when the number of sensor in the array, *M* is changed. In this case, two values for *M* are considered namely, *M*=4 and *M*=6 cases. In Scenario 2, there are two faulty sensors in the array and the number of sensors is *M*=6. Finally, the simulation results are shown as PTD percentages vs. Source angles of the true operating sensor $\boldsymbol{c}$, for the corresponding scenario and number of elements in the array.

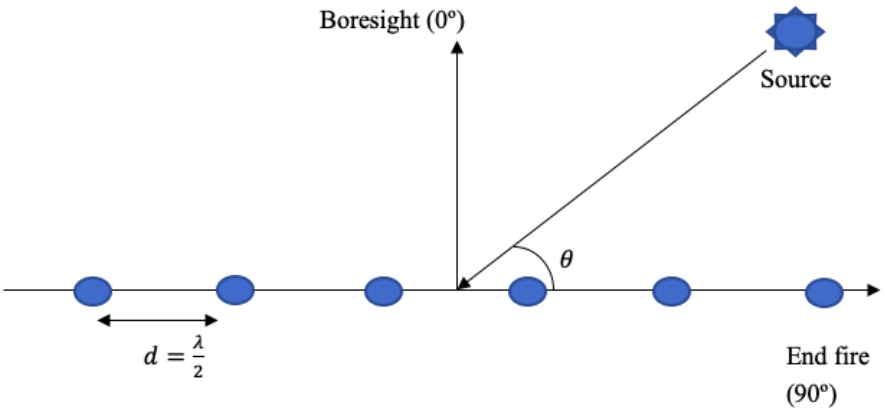

Figure 4.1. Simulation Model

4.1. Scenario 1

4.1.1. $M = 4$

In the case of $M = 4$ array, the results are the same for choosing the faulty sensor from the first and second pairwise sensors due to the symmetry of the array. Hence, the results are given for the faulty sensor existence in the first pairwise sensors. By taking into account the possibility of the faulty sensor existence in the pairwise sensors, simulations are presented for two cases.

The parameters for scenario 1, $M = 4$ for both versions are given in Table 4.1.

Table 4.1. *Parameters for Scenario 1, M=4*

Parameters	*Values*
M (Sensor number)	4
$\boldsymbol{c}$ (operating sensor vector, Case 1)	$[1\ \ 0\ \ 1\ \ 1]^T$
$\boldsymbol{c}$ (operating sensor vector, Case 2)	$[0\ \ 1\ \ 1\ \ 1]^T$
L (Source Number)	1

SNR (dB)	[-10,30]
SNR Resolution (dB)	10
# of Monte Carlo runs	1000
Snapshots	100
Spectral MUSIC Search Angle Resolution (deg)	1
Spectral MUSIC Search Angle	$[-\frac{\pi}{2}, \frac{\pi}{2}]$

The results for Scenario 1 M=4 case is given in Fig. 4.2 and 4.3 respectively for Case 1 and Case 2. As it is expected, PTD gets worse as the SNR is decreased. The distinct feature of these figures is that there is a range of DOA angles where PTD preserves the highest values. It is observed that, for greater SNR values than -10dB, PTD values are %100 for all source angles meaning of faulty sensor detection is valid for a range of DOA angles. When the SNR value is equal to -10dB, the PTD values are low comparing to higher SNR values. However, for the SNR -10dB value, the faulty sensor detection is successful since the PTD values are higher than %80 when the source angle is between 30 and 70 degrees or -30 and -70 degrees. On the contrary, if the source is at the broadside or 0 degrees and at the end-fire or 90, -90 degrees, the faulty sensor cannot be found accurately. Note that, when the source is at the broadside, all the sensors have the same signals. Therefore, it is not possible to find the faulty sensor for this type of observation since faulty sensor channel is the replicate of the healthy sensor channel in our case. In case of end-fire source, array resolution is not good and DOA estimation for ULA is the worst. Hence the accuracy of the faulty sensor detection decreases. While at high SNR, there is a large range of angular sector with accurate detection, for low SNR, the faulty sensor can be detected more accurately between -30 and -70 degrees as well as 30 and 70 degrees.

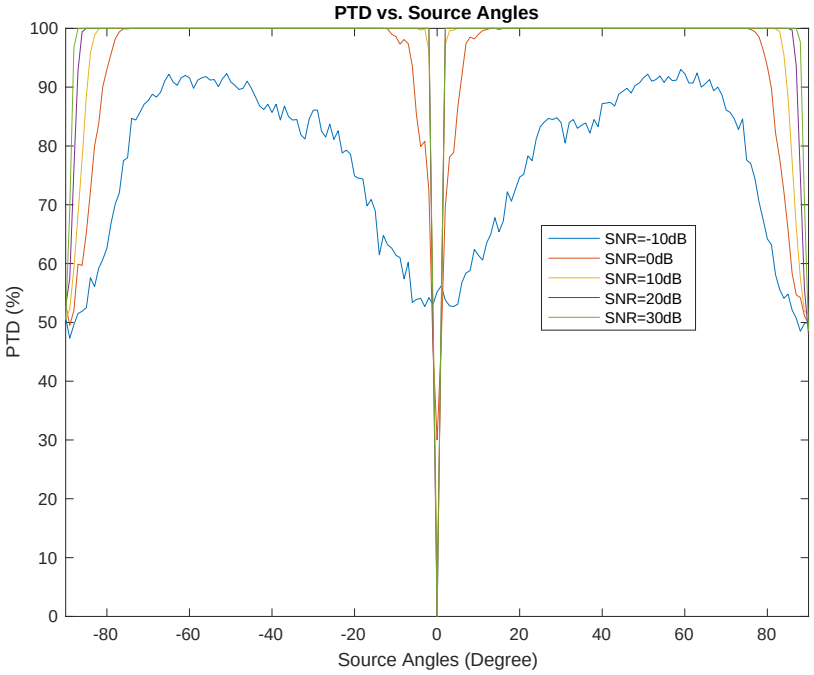

Figure 4.2. PTD of Scenario 1, $M = 4$, Case 1

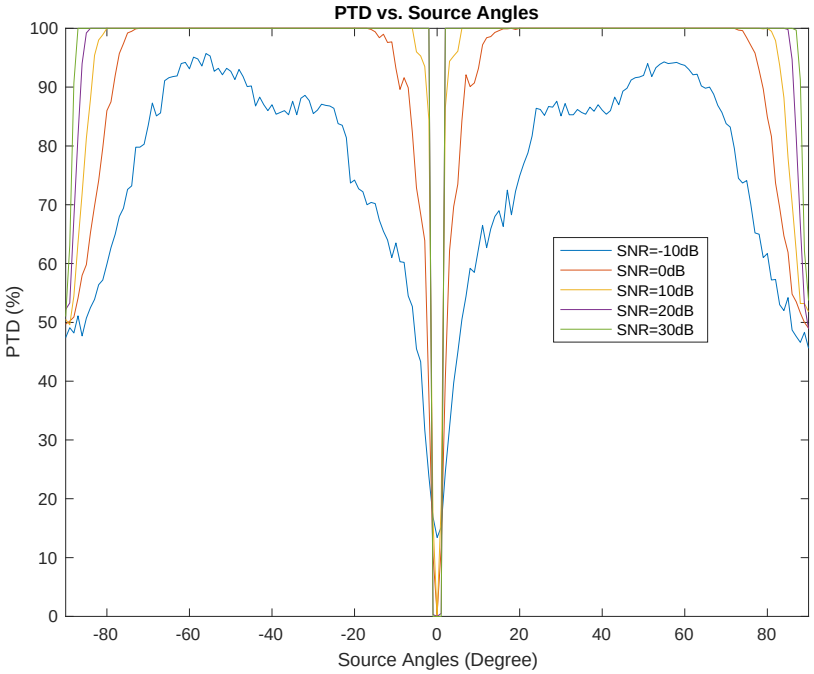

Figure 4.3. PTD of Scenario 1, $M = 4$, Case 2

4.1.2. $M = 6$

In the case of $M = 6$ array, there is only one faulty sensor in the array. This generates a symmetric faulty scenario. For example, faulty sensor existence in the first pairwise sensors generates the same result with faulty sensor existence in the third pairwise sensors. So, the results are given for the faulty sensor exists in the first & second pairwise sensors. Case 1 & 2 are for the faulty sensor existence in the first pairwise sensors and Case 3 & 4 correspond to the faulty sensor existence in the second pairwise sensors.

The parameters for scenario 1, M=6 for all versions are given in Table 4.2.

Table 4.2. *Parameters for Scenario 1, M=6*

Parameters	*Values*
M (Sensor number)	6
$\boldsymbol{c}$ (operating sensor vector, Case 1)	$[1\ 0\ 1\ 1\ 1\ 1]^T$
$\boldsymbol{c}$ (operating sensor vector, Case 2)	$[0\ 1\ 1\ 1\ 1\ 1]^T$
$\boldsymbol{c}$ (operating sensor vector, Case 3)	$[1\ 1\ 0\ 1\ 1\ 1]^T$
$\boldsymbol{c}$ (operating sensor vector, Case 4)	$[1\ 1\ 1\ 0\ 1\ 1]^T$
L (Source Number)	1
SNR (dB)	[-30,10]
SNR Resolution (dB)	10
# of Monte Carlo runs	1000
Snapshots	100
Spectral MUSIC Search Angle Resolution (deg)	1
Spectral MUSIC Search Angle	$[-\frac{\pi}{2}, \frac{\pi}{2}]$

The results of Scenario 1 simulations, PTD percentages of the true array configurations has been shown in Fig. 4.4-4.7. It is observed that, as the number of

sensors increases, angular region where the faulty sensor cannot be detected accurately at the broadside increases. As it is seen from Fig. 4.6, when the source is between -20 and 20 degrees, PTD values are significantly low. This is due to the fact that, the observed output for this angular sector is not sufficient for the resolution of the faulty sensor. Moreover, as the SNR is lowered, the outcome becomes random due to the noise affect.

As a result for Scenario 1 M=6, the best faulty sensor detection angular region is between 40 and 80 degrees or -40 and -80 degrees.

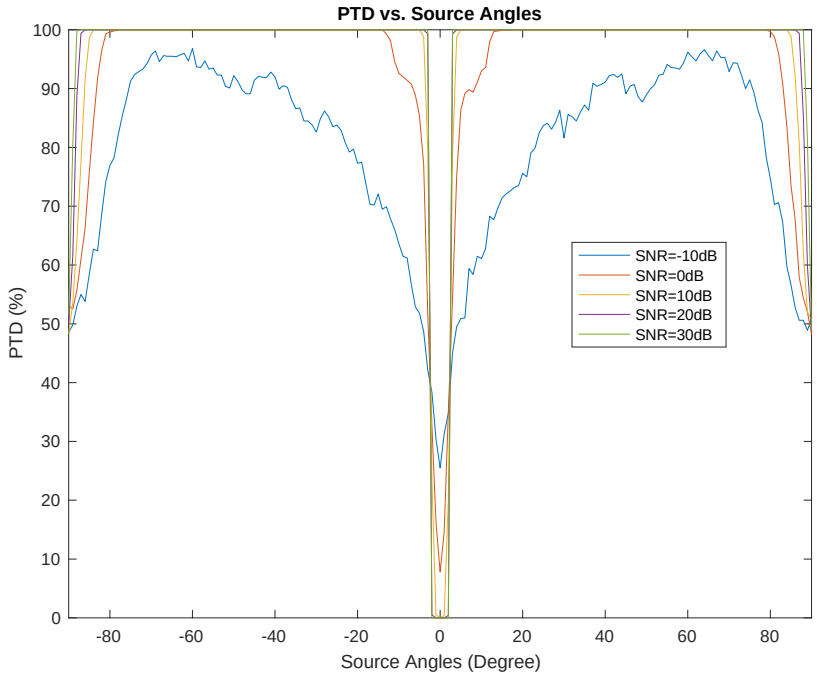

Figure 4.4. PTD of Scenario 1, $M = 6$, Case 1

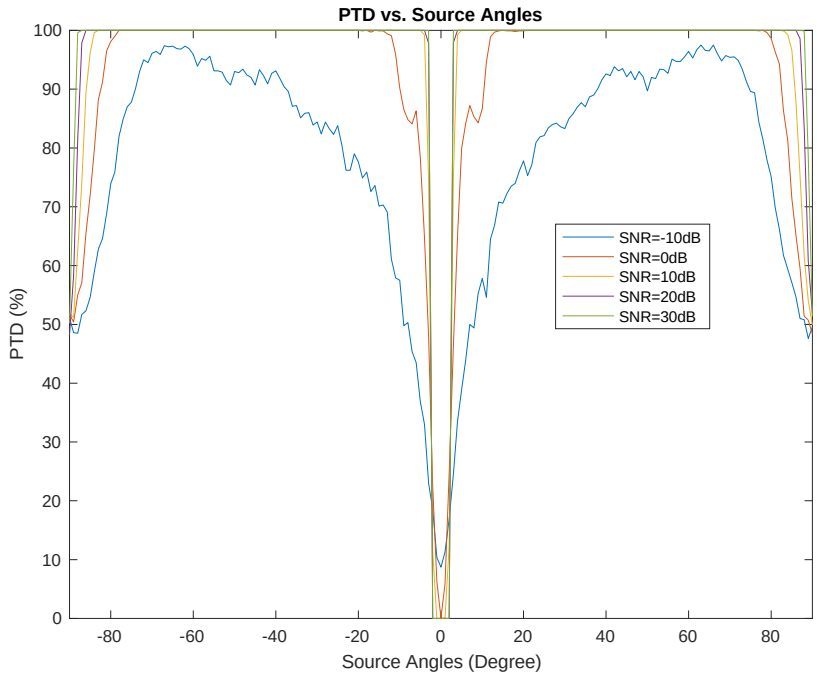

Figure 4.5. PTD of Scenario 1, $M = 6$, Case 2

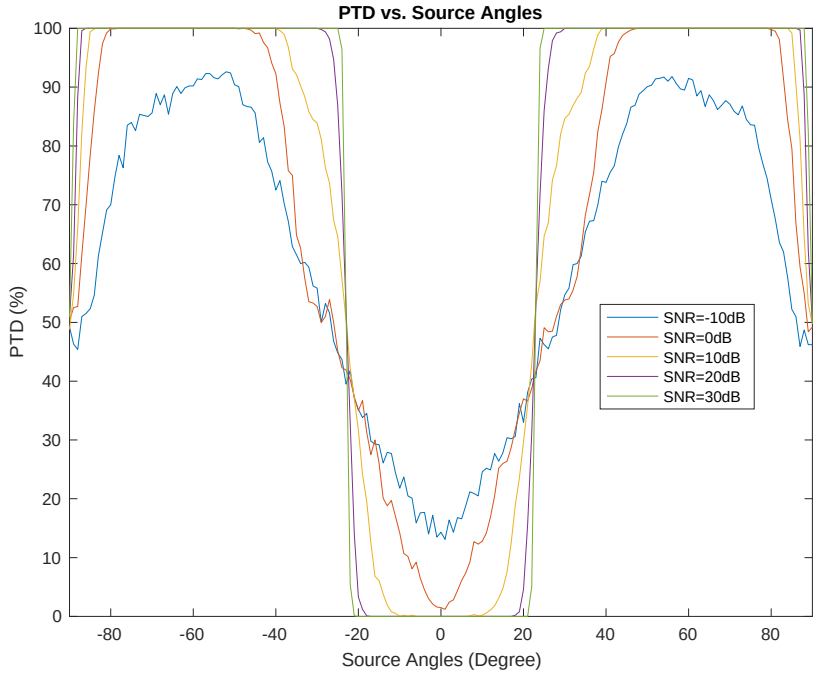

Figure 4.6. PTD of Scenario 1, $M = 6$, Case 3

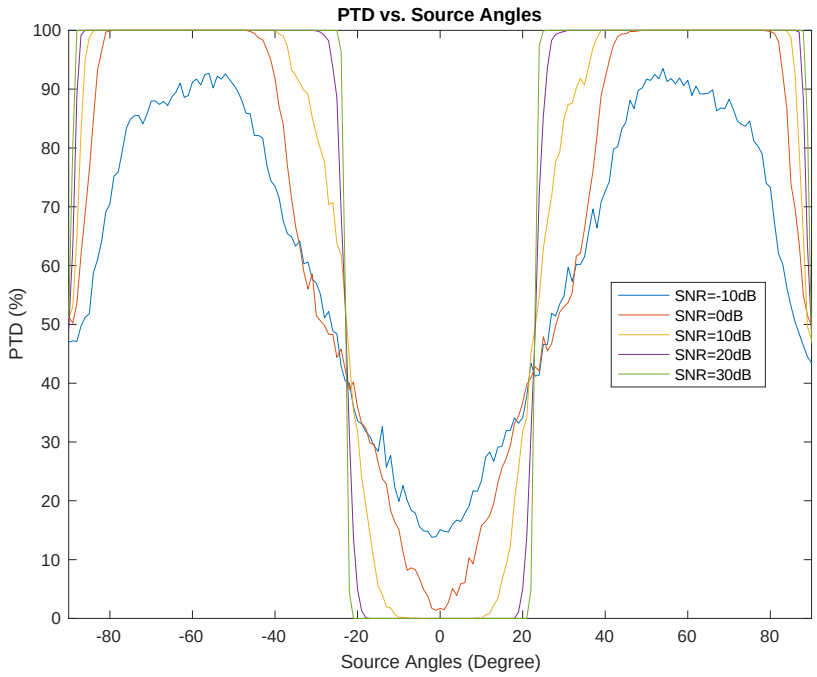

Figure 4.7. PTD of Scenario 1, $M = 6$, Case 4

4.2. Scenario 2

In Scenario 2, for $M = 6$ array, two faulty sensors are existed in two pairwise sensor. Similar with the previous scenario, the symmetry of the array geometry is taking into account for the results. Hence, the results are given for the faulty sensor exists in the first & second and first & third pairwise sensors.

The parameters for Scenario 2, M=6 for all cases are given in Table 4.3.

Table 4.3. *Parameters for Scenario 2, M=6*

Parameters	*Values*
M (Sensor number)	6
$\boldsymbol{c}$ (operating sensor vector, Case 1)	$[1\ 0\ 1\ 0\ 1\ 1]^T$
$\boldsymbol{c}$ (operating sensor vector, Case 2)	$[1\ 0\ 0\ 1\ 1\ 1]^T$
$\boldsymbol{c}$ (operating sensor vector, Case 3)	$[0\ 1\ 1\ 0\ 1\ 1]^T$

$\boldsymbol{c}$ (operating sensor vector, Case 4)	$[0\ 1\ 0\ 1\ 1\ 1]^T$
$\boldsymbol{c}$ (operating sensor vector, Case 5)	$[1\ 0\ 1\ 1\ 0\ 1]^T$
$\boldsymbol{c}$ (operating sensor vector, Case 6)	$[1\ 0\ 1\ 1\ 1\ 0]^T$
$\boldsymbol{c}$ (operating sensor vector, Case 7)	$[0\ 1\ 1\ 1\ 1\ 0]^T$
$\boldsymbol{c}$ (operating sensor vector, Case 8)	$[0\ 1\ 1\ 1\ 0\ 1]^T$
L (Source Number)	1
SNR (dB)	[-30,10]
SNR Resolution (dB)	10
# of Monte Carlo runs	1000
Snapshots	100
Spectral MUSIC Search Angle Resolution (deg)	1
Spectral MUSIC Search Angle	$[-\frac{\pi}{2}, \frac{\pi}{2}]$

For Scenario 2 results, the PTD graphs of true array configurations are presented in Fig 4.7-4.14. First 4 graphs are according to the faulty sensors exist in the first and second pairwise sensors and the following graphs are for the first and third pairwise sensors have the faulty sensors. It is observed that, PTD of Case 7 has the best faulty sensor detection performance at the boresight region of the sensor array. This is because the true array configuration for Case 7 has equal spacing between operating sensor elements, acting like a $M = 4$ ULA. So, the true array configuration has the best DOA performance in the boresight region comparing with other possible array configurations. This phenomenon does not exist for other cases.

Compared to the single faulty sensor case in Fig. 4.6 and 4.7, the angular sector at the broadside where the PTD is low increases in Fig. 4.8. However, for Scenario 2, the best angular region for faulty sensor detection is almost similar to Scenario 1 results, between 40 and 80 degrees of -40 and -80 degrees.

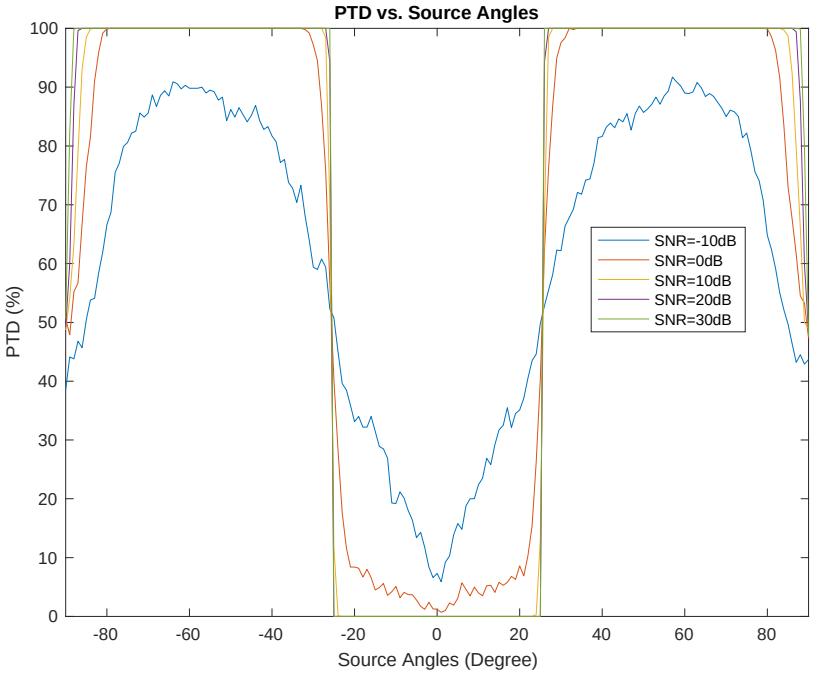

Figure 4.8. PTD of Scenario 2, $M = 6$, Case 1

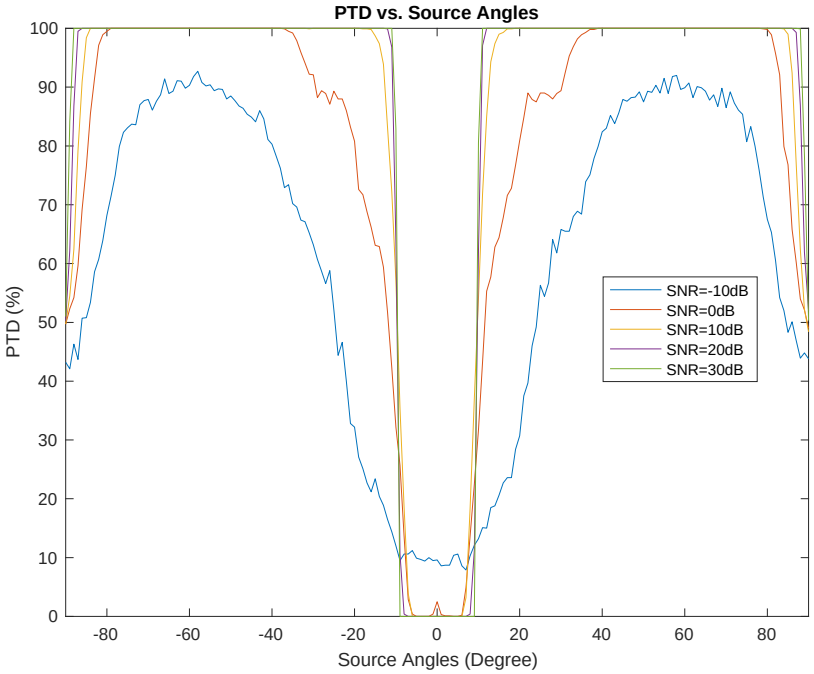

Figure 4.9. PTD of Scenario 2, $M = 6$, Case 2

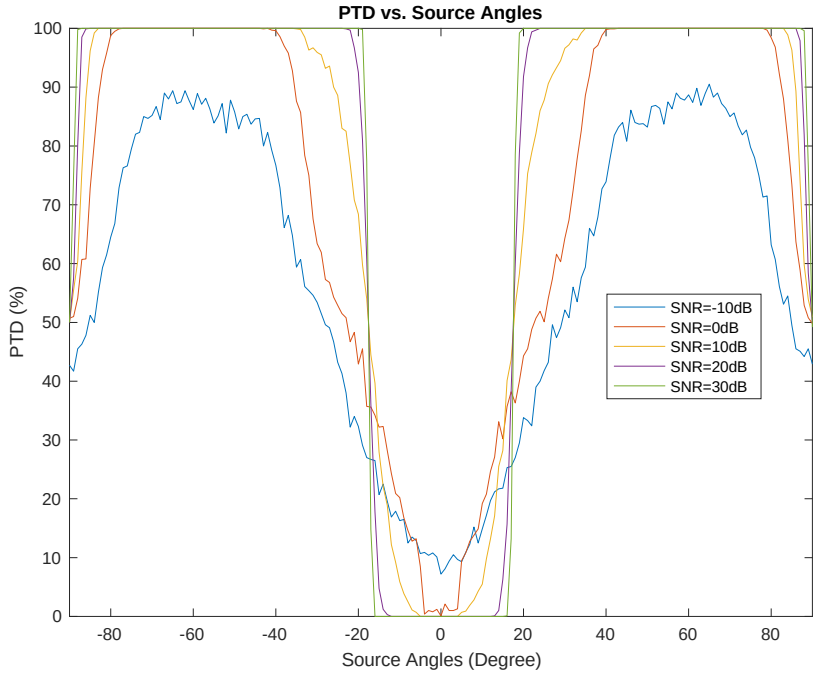

Figure 4.10. PTD of Scenario 2, $M = 6$, Case 3

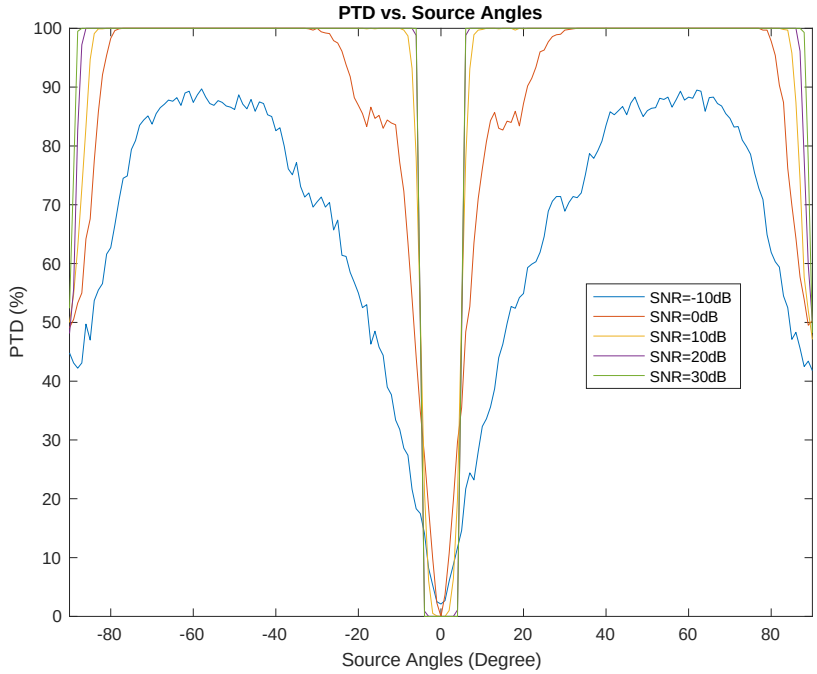

Figure 4.11. PTD of Scenario 2, $M = 6$, Case 4

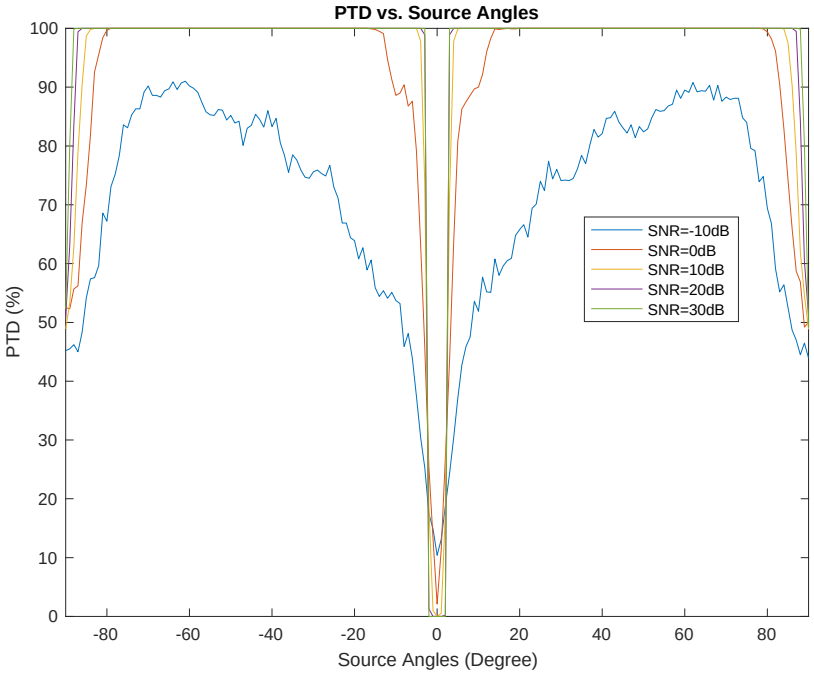

Figure 4.12. PTD of Scenario 2, $M = 6$, Case 5

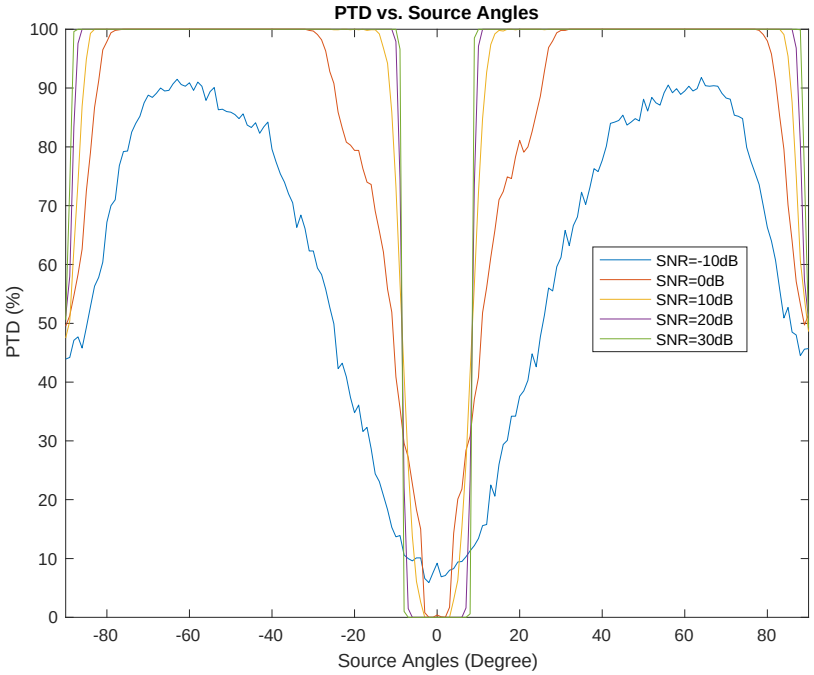

Figure 4.13. PTD of Scenario 2, $M = 6$, Case 6

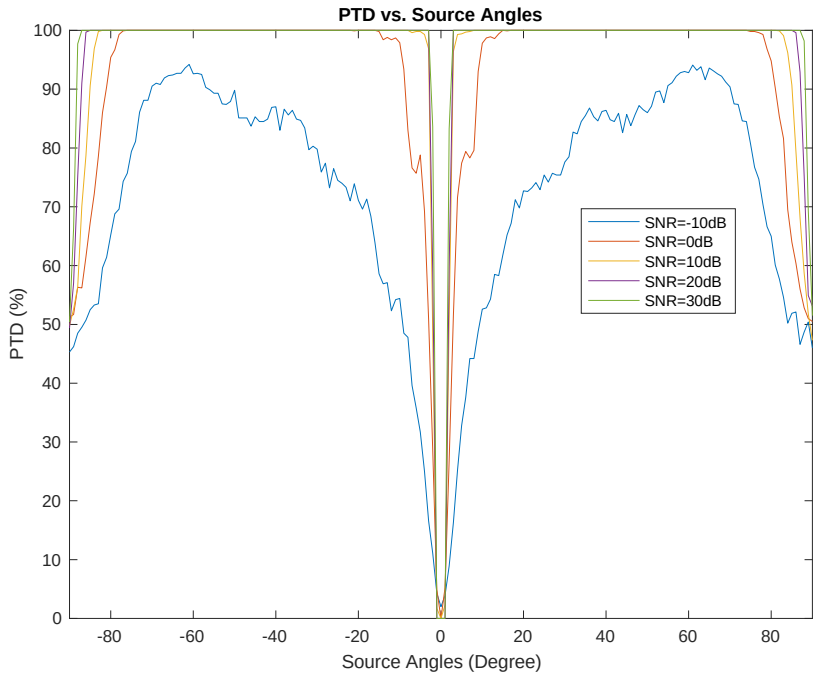

Figure 4.14. PTD of Scenario 2, $M = 6$, Case 7

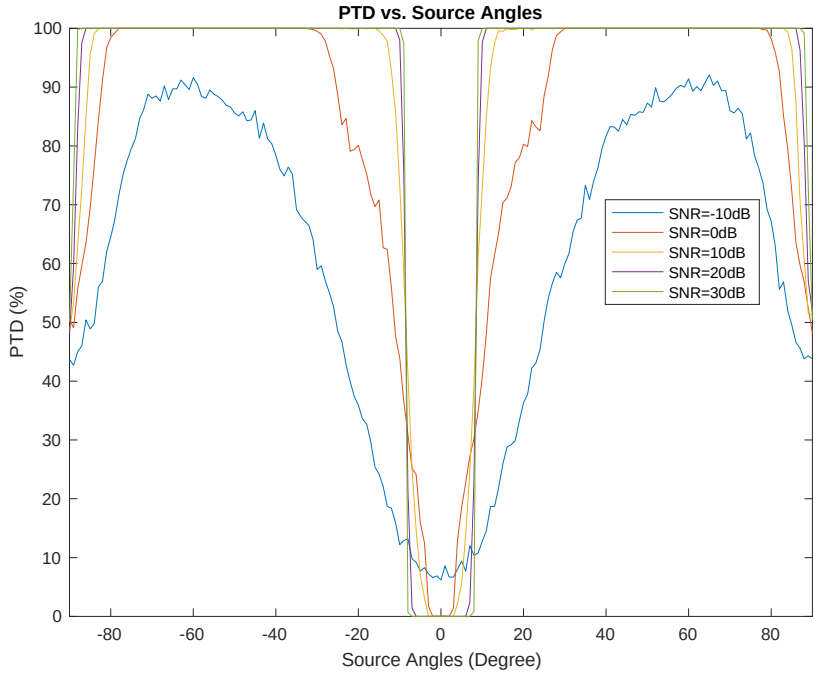

Figure 4.15. PTD of Scenario 2, $M = 6$, Case 8

CHAPTER 5

FAULTY SENSOR DETECTION AND IMPROVED DF ESTIMATION FOR RANDOM ARRAYS

5.1. Problem Definition

In this chapter, the random array problem for faulty sensor is presented and examined. In random array problem, all of the sensors in the array are assumed to be faulty with an associated probability. In other words, the sensors are either operating or not operating according to their operating probability. In the case of the sensor is not operating, output signal is observed as zero. Hence, the received data in random array problem can be named as *randomly missing data*. In the related work for random array in [16], each sensor has the same operating probability. However we enable that each sensor can have different operating possibilities.

Additionally, in random array approach, the operating sensor configuration may differs according to number of snapshots. For example, for a specific number of snapshots the operating sensor configuration remains the same, however for another same number of snapshots it may differs. This is due to the on/off status of sensors changes in a block wise manner. So, detection of faulty sensor can be done for only specific amount of snapshots. As a result, faulty sensors can be detected for specific amount of snapshots in order to prevent the loss of DOA performance.

In deterministic approach, a known DOA source is used in order to detect the faulty MEMS sensors which are produced as pairwise sensors. However, in random array approach, each sensor in the array could be faulty according to the operating probability so proposed method for deterministic approach is not applicable. Nevertheless, a different method is proposed for faulty detection in random arrays.

In order to derive the signal model for random array, ULA signal model and operating probability is used. By considering operating probability p_i and not-operating

probability $1 - p_i$ for each sensor, the operating sensor vector $\boldsymbol{u}$ is obtained in Eqn. 5.1 and 5.2.

$$u_i = \begin{cases} 1, & with\ probability\ p_i \\ 0, & with\ probability\ 1 - p_i \end{cases} \tag{5.1}$$

$$\boldsymbol{u} = [u_1, u_2, \dots, u_M]^T \tag{5.2}$$

The operating sensor vector is used to create the true array steering vector. The true array steering vector is shown in Eqn. 5.3.

$$\tilde{\boldsymbol{a}}(\theta_i) = \boldsymbol{a}(\theta_i) \odot \boldsymbol{u} \tag{5.3}$$

In Eqn. 5.3 $\odot$ represents the Hadamard (element-wise) product. Then, in Eqn. 5.4, array steering matrix containing array steering vectors for each source angle is given.

$$\tilde{\boldsymbol{A}}(\theta) = [\tilde{\boldsymbol{a}}(\theta_1)\ \tilde{\boldsymbol{a}}(\theta_2)\ \tilde{\boldsymbol{a}}(\theta_3) \dots\ \tilde{\boldsymbol{a}}(\theta_L)] \tag{5.4}$$

It can be seen that, the operating probability redefines the array steering vectors, as well as the signal output and covariance matrix in the end. So, the observed signal output becomes as in Eqn. 5.5.

$$\tilde{\boldsymbol{y}}(t) = \tilde{\boldsymbol{A}}(\theta)\boldsymbol{s}(t) + \boldsymbol{n}(t)\ , t = 1, 2, \dots N \tag{5.5}$$

$\boldsymbol{s}(t)$ is the signal waveform with zero mean $E[\boldsymbol{s}(t)] = 0$ and signal power $E[\boldsymbol{s}(t)\boldsymbol{s}^H(t)] = \sigma_s^2 \boldsymbol{I}_M$. The noise is an additive Gaussian white noise with zero mean $E[\boldsymbol{n}(t)] = 0$ and noise power $E[\boldsymbol{n}(t)\boldsymbol{n}^H(t)] = \sigma_n^2 \boldsymbol{I}_M$ covariance matrix. Moreover, noise and signal is assumed to be uncorrelated. Furthermore, the Signal-to-Noise (SNR) can be expressed as

$$SNR = \frac{power\ of\ signal}{power\ of\ noise} = \frac{\sigma_s^2}{\sigma_n^2} \tag{5.6}$$

The important aspect of the random array approach is that, the on/off status of sensors changes in a block wise manner. For example, for the first N_1 snapshots the operating sensor vector remains the same as $\boldsymbol{u_1} = [1\ \ 0\ \ 1\ \ 1]^T$ for 4-element array and for the next N_1 snapshots the operating sensor vector changes as $\boldsymbol{u_2} = [1\ \ 1\ \ 1\ \ 0]^T$.

The covariance matrix is computed as,

$$\boldsymbol{R} = E[\tilde{\boldsymbol{y}}(t)\tilde{\boldsymbol{y}}^H(t)] = \tilde{\boldsymbol{A}}(\theta)\boldsymbol{s}(t)\boldsymbol{s}^H(t)\tilde{\boldsymbol{A}}^H(\theta) + \boldsymbol{n}(t)\boldsymbol{n}^H(t) \tag{5.7}$$

$$\boldsymbol{R} = \sigma_s^2\tilde{\boldsymbol{A}}(\theta)\tilde{\boldsymbol{A}}^H(\theta) + \sigma_n^2\boldsymbol{I}_M \tag{5.8}$$

The array steering matrix in Eqn. 5.8 contains all steering vectors for L sources as in Eqn.2.17.

Derivation of the signal subspace eigenvalues formulation is critical for random array case since it is used in the proposed method for faulty sensor detection. Hence, the covariance matrix formulation is derived in Eqn. 5.9 for single source case $L = 1$.

$$\boldsymbol{R} = \begin{bmatrix} \sigma_s^2 u_1^2|\tilde{a}_1|^2 + \sigma_n^2 & u_1u_2\tilde{a}_1\tilde{a}_2^H & \cdots & u_1u_M\tilde{a}_1\tilde{a}_M^H \\ u_1u_2\tilde{a}_2\tilde{a}_1^H & \sigma_s^2 u_2^2|\tilde{a}_2|^2 + \sigma_n^2 & \cdots & u_2u_M\tilde{a}_2\tilde{a}_M^H \\ \vdots & \vdots & \ddots & \vdots \\ u_1u_M\tilde{a}_M\tilde{a}_1^H & u_2u_M\tilde{a}_2\tilde{a}_M^H & \ldots & \sigma_s^2 u_M^2|\tilde{a}_M|^2 + \sigma_n^2 \end{bmatrix} \tag{5.9}$$

where $\tilde{\boldsymbol{a}}(\theta) = [\tilde{a}_1\ \ \tilde{a}_2\ \ \ldots\ \ \tilde{a}_M]^T$.

Eigenvalues of the covariance matrix are obtained as,

$$\boldsymbol{R} = \boldsymbol{V}\boldsymbol{\Lambda}\boldsymbol{V}^H\ ,\ \boldsymbol{\Lambda} = diag\{\lambda_1, \lambda_2, \ldots, \lambda_M\} \tag{5.10}$$

$$\sum_{i=1}^{M} \lambda_i = \sigma_s^2 \sum_{i=1}^{M} u_i^2 |a_i|^2 + M\sigma_n^2 \tag{5.11}$$

Since $L = 1$, single source, $\lambda_2 = \cdots = \lambda_M = \sigma_n^2$, by considering the eigenvalues are in a descending order. Moreover, $|\tilde{a}_i|^2 = 1$. By rewriting Eqn. 5.11it is obtained that,

$$\lambda_1 = \sigma_s^2 \sum_{i=1}^{M} u_i^2 + \sigma_n^2 = \sigma_s^2 M' + \sigma_n^2 \tag{5.12}$$

where M' is the number of operating sensors which $M' \leq M$.

For multiple source case, $L > 1$, the covariance matrix is given in Eqn. 5.13. Moreover, by applying the same steps with the single source case, Eqn. 5.14 is obtained.

$$\boldsymbol{R} = \begin{bmatrix} \sigma_s^2 u_1^2 \sum_{i=1}^{L} |\widetilde{\boldsymbol{A}}_{i,1}|^2 + \sigma_n^2 & u_1 u_2 \sum_{i=1}^{L} \widetilde{\boldsymbol{A}}_{i,1} \widetilde{\boldsymbol{A}}_{i,2}^* & \cdots & u_1 u_M \sum_{i=1}^{L} \widetilde{\boldsymbol{A}}_{i,1} \widetilde{\boldsymbol{A}}_{i,M}^* \\ u_1 u_2 \sum_{i=1}^{L} \widetilde{\boldsymbol{A}}_{i,2} \widetilde{\boldsymbol{A}}_{i,1}^* & \sigma_s^2 u_2^2 \sum_{i=1}^{L} |\widetilde{\boldsymbol{A}}_{i,2}|^2 + \sigma_n^2 & \cdots & u_2 u_M \sum_{i=1}^{L} \widetilde{\boldsymbol{A}}_{i,2} \widetilde{\boldsymbol{A}}_{i,M}^* \\ \vdots & \vdots & \ddots & \vdots \\ u_1 u_M \sum_{i=1}^{L} \widetilde{\boldsymbol{A}}_{i,M} \widetilde{\boldsymbol{A}}_{i,1}^* & u_2 u_M \sum_{i=1}^{L} \widetilde{\boldsymbol{A}}_{i,M} \widetilde{\boldsymbol{A}}_{i,2}^* & \cdots & \sigma_s^2 u_M^2 \sum_{i=1}^{L} |\widetilde{\boldsymbol{A}}_{i,M}|^2 + \sigma_n^2 \end{bmatrix} \tag{5.13}$$

$$\sum_{i=1}^{M} \lambda_i = \sigma_s^2 \sum_{i=1}^{M} u_i^2 \sum_{l=1}^{L} \left|\boldsymbol{A}_{i,l}\right|^2 + M\sigma_n^2 \tag{5.14}$$

In Eqn. 5.14, the left side can be arranged since $\lambda_{L+1} = \lambda_{L+2} = \cdots = \lambda_M = \sigma_n^2$, by considering the eigenvalues are in a descending order. Moreover, $\left|\boldsymbol{A}_{i,l}\right|^2 = 1$. By rewriting Eqn. 5.14 it is obtained that,

$$\sum_{i=1}^{L} \lambda_i = \sigma_s^2 L \sum_{i=1}^{M} u_i^2 + L\sigma_n^2 = \sigma_s^2 M' L + \sigma_n^2 L = L(\sigma_s^2 M' + \sigma_n^2) \tag{5.15}$$

As it can be seen by comparing Eqn. 5.15 and 5.12, sum of the multiple case signal subspace eigenvalues turns out to be equal to L times of the single source signal subspace eigenvalue. Therefore, the problem is to find the faulty sensors given the array output or covariance matrix. In the following part, the problem is solved by using the signal subspace formulation above and MUSIC-based DOA estimation methods.

5.2. Problem Solution

The aim is to improve DOA estimation performance that degraded due to faulty sensors, randomly missing data. There are related works for DOA estimation with randomly missing data, for example MUSIC performance analysis with randomly missing data [17]. Moreover, it is stated that MUSIC algorithm is not *M, N*-consisted in [26] where it fails to provide consistent estimates in the general asymptotic regime. Therefore, G-MUSIC algorithm is introduced in [24] with its performance analysis with random linear array in [27]. The purpose of applying G-MUSIC method is that, consistent DOA estimation is valid without detecting faulty sensors in the array. In addition, MUSIC and G-MUSIC randomly missing data studies use the whole sensor array without distinguishing operating and not operating sensors. However, by detecting and eliminating the faulty sensors, better DOA performance is achievable where our motivation lies on.

In the following proposed method for random array approach steps are introduced.

5.2.1. Step1: Estimating signal and noise powers

Since the sum of signal subspace eigenvalues has been known from Eqn. 5.12 and 5.15, both for single and multiple source cases, number of operating sensors can be

found by estimating the SNR value. However, the signal and noise powers must be found in order to estimate an accurate SNR value.

By taking the diagonal elements of the received signal covariance matrix in Eqn. 5.9, the output signal powers can be found for each sensor. Since some sensors do not operate at all according to the associated operating probability, the channel signals for them are composed of only noise. According to the sensor operating or faulty status, the output signal power for each sensor is equal to either only noise power or sum of signal and noise power as in Eqn. 5.16.

$$\boldsymbol{R}_{ii} = E[\boldsymbol{y}_i(t) * \boldsymbol{y}_i^*(t)] = \sigma_s^2 u_i^2 |\tilde{a}_i|^2 + \sigma_n^2 \tag{5.16}$$

Detection of faulty sensors can be made through comparing the received signal powers for each sensor since output power of operating sensors are greater than faulty sensors' as in Eqn. 5.16. It possible to distinguish the received powers according to their amplitudes by using a threshold value. However, for different SNR values the threshold value must differ. Hence, instead of using a threshold method, k-means projective clustering method [28] which seeks to minimize the average squared distance between points in the same cluster, is applied. K-means clustering method is fast, effective and has the ability to choose cluster dimension. Furthermore, the received signal powers are divided into two partitions as received signals of operating and not-operating sensors by using k-means clustering method. However, for low SNR, k-means clustering method would not work properly since the power values are not easily distinguished. So, some modifications have been added to the clustering step.

5.2.2. Step2: Estimating number of operating sensors

In addition to the output of the clustering step, SNR is found by using the estimates of operating and not-operating sensors. The distinguished operating sensor received signals from k-means clustering output are denoted as $\boldsymbol{y}_{op}$ and not-operating received

signals as $\boldsymbol{y}_{nop}$. By taking the average of the received signals of operating and not operating sensors in Eqn.5.17 and 5.18, the signal and noise powers are found.

$$\hat{\sigma}_n^2 = \frac{1}{N * M_{nop}} \sum_{i=1}^{M_{no}} \sum_{t=1}^{N} \boldsymbol{y}_{nop,i}(t) * \boldsymbol{y}_{nop,i}^*(t) \tag{5.17}$$

$$\hat{\sigma}_s^2 = \frac{1}{N * M_{no}} \sum_{i=1}^{M_o} \sum_{t=1}^{N} \boldsymbol{y}_{op,i}(t) * \boldsymbol{y}_{op,i}^*(t) - \hat{\sigma}_n^2 \tag{5.18}$$

$$SNR = \frac{\hat{\sigma}_s^2}{\hat{\sigma}_n^2} \tag{5.19}$$

where M_{op} refers to the number of operating sensors and M_{nop} refers to the number of faulty, not operating sensors found from the clustering step.

In Eqn. 5.20 and 5.21, the possible number of operating sensors can be found by using the eigenvalue formulations derived in Eqn. 5.12.

$$\widehat{M}_1{}' = \left\lfloor \underset{M'}{\operatorname{argmin}} \lambda_1 - (M'\sigma_s^2 + \sigma_n^2) \right\rfloor, \qquad M' \in [1, M] \tag{5.20}$$

$$\widehat{M}_2' = \left\lfloor \underset{M'}{\operatorname{argmin}} \lambda_1 - (M'\sigma_s^2 + \sigma_n^2) \right\rfloor, \qquad M' \in [1, M] \tag{5.21}$$

Since the solution of the same cost function in Eqn. 5.20 and 5.21 is not an integer value, both solutions are rounded up and down. Rounded solutions are considered as possible number of operating sensors, $\widehat{M}_1'$, $\widehat{M}_2'$. Rounding operation also enables us to prevent wrong estimations as possible as it can. It should be noted that, especially in low SNR cases, taking only the rounded up estimation of the minimization solution, do not provide efficient performances.

5.2.3. Step3: Constructing possible array configurations

By using the estimates of the $\widehat{M}'$values, the possible sensor array configurations can be constructed with using all permutations of operating sensor vector. For example, consider a $M = 4$ sensor array with first and the third sensors are faulty. The estimates for the operating sensor numbers are 2 & 3. The possible array steering matrices are constructed as Eqn. 5.22 by using the possible operating sensor vectors in Eqn. 5.23.

$$\tilde{\boldsymbol{a}}_i = \boldsymbol{a} \odot \tilde{\boldsymbol{u}}_i \tag{5.22}$$

$$\begin{aligned}
\tilde{\boldsymbol{u}}_1 &= [1\ \ 1\ \ 0\ \ 0]^T \\
\tilde{\boldsymbol{u}}_2 &= [1\ \ 0\ \ 1\ \ 0]^T \\
\tilde{\boldsymbol{u}}_3 &= [1\ \ 0\ \ 0\ \ 1]^T \\
\tilde{\boldsymbol{u}}_4 &= [0\ \ 0\ \ 1\ \ 1]^T \\
\tilde{\boldsymbol{u}}_5 &= [0\ \ 1\ \ 0\ \ 1]^T \\
\tilde{\boldsymbol{u}}_6 &= [0\ \ 1\ \ 1\ \ 0]^T \\
\tilde{\boldsymbol{u}}_7 &= [0\ \ 1\ \ 1\ \ 1]^T \\
\tilde{\boldsymbol{u}}_8 &= [1\ \ 0\ \ 1\ \ 1]^T \\
\tilde{\boldsymbol{u}}_9 &= [1\ \ 1\ \ 0\ \ 1]^T \\
\tilde{\boldsymbol{u}}_{10} &= [1\ \ 1\ \ 1\ \ 0]^T
\end{aligned} \tag{5.23}$$

Where the actual $\boldsymbol{u}$ vector is $\boldsymbol{u} = [0\ \ 1\ \ 0\ \ 1]^T$.

Number of possible array configurations can be found $P_u = \binom{M}{\widehat{M}_1'} + \binom{M}{\widehat{M}_2'}$ as according to the two minimum solutions of the minimization of the cost in Eqn. 5.20 and 5.21.

5.2.4. Step4: Detection of Faulty Sensors and DOA Estimation

In this part of the proposed method, both Root-MUSIC and Spectral MUSIC are used in order to comparing the possible array configurations DOA outputs to estimate the correct one. The reason for using both Root and Spectral MUSIC, is to have less computation in high performances. Although it is possible to use only one of methods among the Spectral and Root-MUSIC, it leads us to computational or performance problems.

In Root-MUSIC application step, all the possible array steering matrices, $\widetilde{\boldsymbol{a}}_i$'s, are used in order to estimate the DOAs respectively. Since there may be faulty, not operating sensors, Root-MUSIC for NLA is used which is presented in Chapter 2. At the end, the DOAs for each possible array configuration will be estimated as $\hat{\theta}_{root,i}$.

$$\hat{\theta}_{root,i} = \sin^{-1}\left(\frac{\varphi_{\hat{z}_i}\lambda}{2\pi d}\right) \tag{5.24}$$

In the following, the correct array configuration is detected, resulting with faulty sensors detection for specific amount of snapshots N. DOA estimates of Root-MUSIC for each possible array configurations are substituted in MUSIC spectrum formulation in Eqn. 5.25. Since the best DOA estimation must have the highest MUSIC cost value, DOA estimate among the possibilities which has the maximum cost is chosen as the correct one where the true array configuration is the corresponding $\widehat{\boldsymbol{u}}$ vector. Furthermore, faulty sensors can be detected, where they are represented as 0 (zero) values in the $\widehat{\boldsymbol{u}}$'s.

$$p_{music,i}\left(\hat{\theta}_{root,i}\right) = \frac{1}{\boldsymbol{A}^H\left(\hat{\theta}_{root,i}\right)\boldsymbol{G}\boldsymbol{G}^H\boldsymbol{A}\left(\hat{\theta}_{root,i}\right)} \tag{5.25}$$

$$\hat{\theta} = \max_i \left| p_{music,i}\left(\hat{\theta}_{root,i}\right) \right| \tag{5.26}$$

Detection of the faulty sensors, in other words correct array configuration estimation can be done by using the roots of the Root-MUSIC polynomial equation. This can be achieved by comparing the distances of the estimate roots to the unit circle for each possible array configuration and taking the closest one to the unit circle. However, DOA performance of using only Root-MUSIC for random array approach is not good as the proposed algorithm performance. Furthermore, detection of faulty sensors can

be established by using only Spectral MUSIC either. Although the performance will be the same with the proposed method performance, computational complexity will grow ending with a slower algorithm.

Special Case: All Sensors Operating

Since each sensor's fault is associated with probability, it is possible that all sensors are in operating mode according to the value of the probability. In the proposed method, the operating and not-operating sensors are founded by using k-means clustering algorithm. Although the clustering procedure is for distinguishing the received signal powers to find the operating and faulty sensors, when all sensors are operating clustering output could not be correct since it divides the received signal powers into two clusters according to power levels. Nevertheless, the modification step after the k-means clustering solves the problem.

After k-means clustering step, signal and noise powers are estimated in the proposed method. Since the received signal for each sensor contains both signal and noise power, the estimated powers will be not correct according to false clustering operating status output. The estimated noise power is computed higher than it should be, therefore signal power is computed less than the right ones in Eqn. 5.17 and 5.18. Computation steps are presented in Eqn. 5.27 and 5.28.

$$\hat{\sigma}_n^2 = \sigma_n^2 + \sigma_n^2 - \in \tag{5.27}$$

$$\hat{\sigma}_s^2 = \sigma_s^2 + \sigma_n^2 - \hat{\sigma}_n^2 = \in \tag{5.28}$$

where $\in$ is positive infinitesimal quantity and the value varies according to the snapshot number and SNR value. The noise power term is computed slightly smaller than the received signal power due to the clustering outputs based on received signal power. Since the estimated signal power is computed as a very small quantity, the

outputs of Eqn. 5.20 and 5.21 will be equal to M and $M-1$ respectively. As a result, even though estimating false signal and noise powers, number of operating sensors could be computed correctly especially in high SNR values.

Detection of Faulty Sensors and Improved DOA Algorithm In Practical Applications

- Compute the SCM

$$\widehat{\boldsymbol{R}} = \frac{1}{N}\sum_{t=1}^{N} \tilde{\boldsymbol{y}}(t)\tilde{\boldsymbol{y}}^{H}(t) \tag{5.29}$$

- Apply k-means clustering method to the diagonal terms of SCM in order to find operating and not-operating sensors by clustering the received signal powers from SCM

$$diag\{\widehat{\boldsymbol{R}}_{ii}\} = \sigma_s^2 p_i^2 |a_i|^2 + \sigma_n^2 \tag{5.30}$$

- Find signal, noise powers and SNR from clustering outputs

$$\hat{\sigma}_n^2 = \frac{1}{N * M_{no}} \sum_{i=1}^{M_{no}} \sum_{t=1}^{N} \tilde{\boldsymbol{y}}_{nop,i}(t) * \tilde{\boldsymbol{y}}_{nop,i}^{*}(t) \tag{5.31}$$

$$\hat{\sigma}_s^2 = \frac{1}{N * M_o} \sum_{i=1}^{M_o} \sum_{t=1}^{N} \tilde{\boldsymbol{y}}_{op,i}(t) * \tilde{\boldsymbol{y}}_{op,i}^{*}(t) - \hat{\sigma}_n^2 \tag{5.32}$$

$$\widehat{SNR} = \frac{\hat{\sigma}_s^2}{\hat{\sigma}_n^2} \tag{5.33}$$

- Find the signal and noise subspace eigenvalues and eigenvectors by using the eigen decomposition of SCM

$$\lambda_1 \geq \lambda_2 \geq \cdots \geq \lambda_L \geq \lambda_{L+1} \geq \cdots \geq \lambda_M \tag{5.34}$$

$$\widehat{\boldsymbol{G}} = [\widehat{\boldsymbol{g}}_1, \widehat{\boldsymbol{g}}_2, \ldots, \widehat{\boldsymbol{g}}_L] \tag{5.35}$$

- Find two estimates of number of operating sensors that gives minimum two costs in the below.

$$\widehat{M_1}' = \underset{M'}{\operatorname{argmin}}\lceil \lambda_1 - (M'\sigma_s^2 + \sigma_n^2)\rceil \tag{5.36}$$

$$\widehat{M_2'} = \underset{M'}{\operatorname{argmin}}\lfloor \lambda_1 - (M'\sigma_s^2 + \sigma_n^2)\rfloor \tag{5.37}$$

- According to the number of operating sensor estimates, $\widehat{M_i}'$, construct the possible array steering matrices configurations, $\widetilde{\boldsymbol{a}}_i$.

- Estimate DOAs with Root-MUSIC algorithm for each possible array configuration.

$$\hat{\theta}_{root,i} = \sin^{-1}\left(\frac{\varphi_{\hat{z}_i}\lambda}{2\pi d}\right) \tag{5.38}$$

- Substitute the estimated DOAs with Root-MUSIC method into the Spectral MUSIC cost function.

$$p_{music,i}\left(\hat{\theta}_{root,i}\right) = \frac{1}{\boldsymbol{A}^H\left(\hat{\theta}_{root,i}\right)\boldsymbol{G}\boldsymbol{G}^H\boldsymbol{A}\left(\hat{\theta}_{root,i}\right)} \tag{5.39}$$

- Compare the Spectral MUSIC costs for each possible array configuration, find the minimum value respectively with the array configuration and estimated DOA.

$$\hat{\theta} = \max_i |p_{music}(\hat{\theta}_{root,i})| \tag{5.40}$$

- Detect the faulty sensors from the estimated DOA corresponding $\widehat{\boldsymbol{u}}$

CHAPTER 6

RESULTS OF FAULTY SENSOR DETECTION AND IMPROVED DF ESTIMATION FOR RANDOM ARRAYS

In this part of the thesis, results for the random array approach have been given. In the simulations, the improved estimation method is compared with other DOA estimation algorithms in performance criteria. Furthermore, the comparisons are done for different scenarios, probability values, snapshots and sensor element numbers. In the given graphs, the DOA estimation RMSE (Root Mean Square Error) values are compared for different DOA methods and PTD of faulty sensor detection graphs for the proposed method are presented.

The comparison has been made through firstly with Spectral and Root-MUSIC with the correct operating sensors. This is taken as a reference since in the random array problem operating sensors are not known. Furthermore, Spectral MUSIC and G-MUSIC are used for comparison where these methods are using the whole array sensors without the knowledge of the operating array steering vectors. Lastly, the proposed estimation method is demonstrated.

The simulations for random array approach divides into two parts, single source case and multiple source cases.

The description of the legends of the graphs are as:

MUSIC Real Configuration: Spectral MUSIC with correct operating sensors

Root MUSIC Real Conf: Root-MUSIC with correct operating sensors

MUSIC RLA: Spectral MUSIC by using all sensors in random linear array

G-MUSIC RLA: G-MUSIC by using all sensors in random linear array

Improved RLA: Proposed algorithm for RLA, hybrid Spectral and Root-MUSIC

Operating possibilities for each sensor is represented as p_i. In the case of equal probabilities for each sensor is considered, operating possibility is shown as p. If each sensor has different operating possibility, it is denoted by operating probability vector, $\boldsymbol{u}$.

6.1. Single Source Case

6.1.1. $M = 6$

First consider $M = 6$, and the all sensors are operating as probability of $p = 0.8$. Element spacing between the sensors in the array is chosen as $d = \frac{\lambda}{10}$ in order to preventing aliasing problem by fitting the array in $\frac{\lambda}{2}$. Angle of the source is chosen as 25° in the simulations.

Table 6.1. Single Source Case, M=6, p=0.8

Parameters	*Values*
M (Sensor number)	6
p (Operating sensor possibility)	0.8
L (Source Number)	1
SNR (dB)	[-5,10]
SNR Resolution (dB)	5
# of Monte Carlo runs	1000
N (Snapshots)	10, 50, 100
Spectral MUSIC Search Angle Resolution (deg)	0.1
AOA of Source Angle	25°
Spectral MUSIC Search Angle	[0º, 90º]

The results are given in Fig 6.1 – 6.3 and presenting the DOA estimation performances of the methods for different number of snapshots and SNR values in the manner of RMS Error in degrees. Additionally, the PTD percentages of proposed method faulty sensor detection for various SNR and number of snapshots are shown in Fig 6.4 Since two methods, Spectral and Root-MUSIC with real array configuration, using the correct operating sensors in their DOA estimation problem, performances are optimum that can be taken as a reference. Although, the proposed method does not use the correct array configuration, method's performance converges to the optimum as snapshot and SNR gets higher. This is due to PTD of faulty sensor detection reaches %100 at 0dB SNR, meaning of detecting the faulty sensor in every trial, for 50 and 100 snapshots as it can be observed from Fig 6.4. On the contrary of the proposed method, MUSIC and G-MUSIC methods are using all sensors in the array for DOA estimation. Therefore, they do not achieve optimum performances. Also, MUSIC and G-MUSIC algorithm performances are nearly the same. It should be noted that, the proposed method has significantly better DOA performance than MUSIC and G-MUSIC for M=6, p=0.8 case. Additionally, the proposed method can detect the faulty sensor and sensors accurately according to the SNR and number of snapshots.

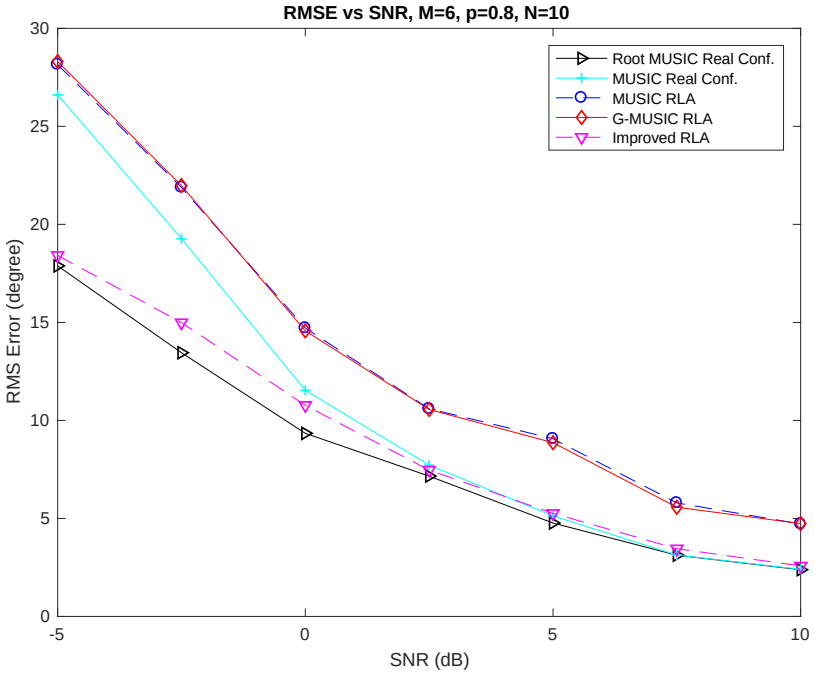

Figure 6.1. RMSE vs SNR, *M*=4, p=0.8, N=10

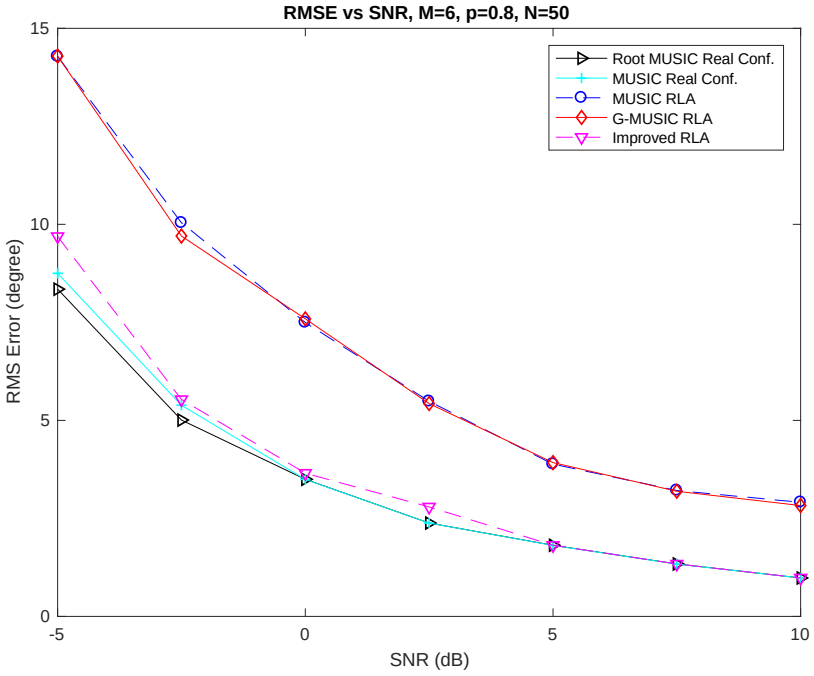

Figure 6.2. RMSE vs SNR, *M*=4, p=0.8, N=50

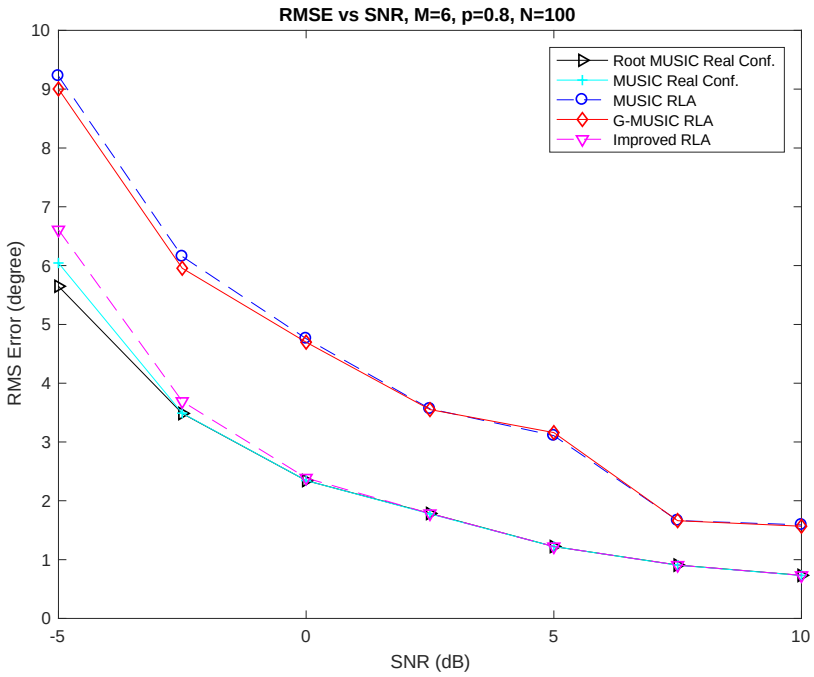

Figure 6.3. RMSE vs SNR, *M*=4, p=0.8, N=100

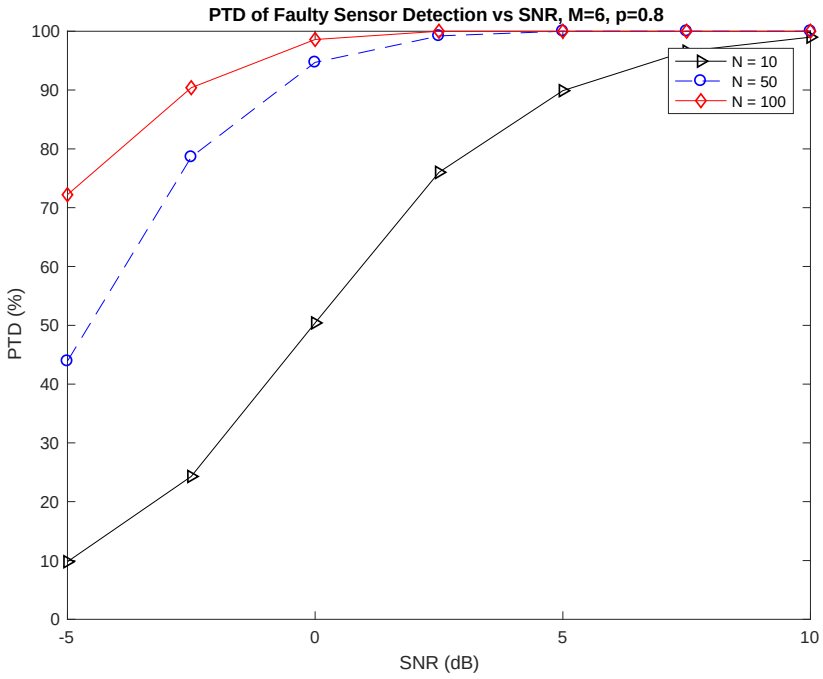

Figure 6.4. PTD of Faulty Sensor Detection vs SNR, *M*=4, p=0.8

6.1.2. $M = 6$ Different Sensor Possibilities

In this case, each sensor in the array has different operating possibility that operating sensor vector becomes as, $\boldsymbol{u} = [0.8\ 0.9\ 0.7\ 0.6\ 0.8\ 0.9]^T$. Element spacing between the sensors in the ULA array is chosen as $d = \frac{\lambda}{10}$ in order to prevent the aliasing problem by fitting the array in $\frac{\lambda}{2}$. The source angle is 25º similar with the previous case.

Table 6.2. Single Source Case, M=6, $\boldsymbol{u} = [0.8\ 0.9\ 0.7\ 0.6\ 0.8\ 0.9]^T$

Parameters	*Values*
M (Sensor number)	6
$\boldsymbol{u}$ (Operating sensor possibility vector)	$[0.8\ 0.9\ 0.7\ 0.6\ 0.8\ 0.9]^T$
L (Source Number)	1
SNR (dB)	[-5,10]
SNR Resolution (dB)	5
# of Monte Carlo runs	1000
N (Snapshots)	10, 50, 100
Spectral MUSIC Search Angle Resolution (deg)	0.1
AOA of Source Angle	25°
Spectral MUSIC Search Angle	[0º, 90º]

Different operating probabilities for each sensor enables us to show the robustness ability of the proposed method. Since the problem formulation is according to the number of operating sensors, giving different probabilities for each sensor does not affect the performance of the proposed method. Results of RMSE performance graphs are given in Fig 6.5-6.7 with comparing the methods. Even in low SNR value and number of snapshots, improved method has better performance than MUSIC and G-

MUSIC for M=6, $\mathbf{u} = [0.8 \;\; 0.9 \;\; 0.7 \;\; 0.6 \;\; 0.8 \;\; 0.6]^{\mathrm{T}}$ case. Due to the detection of faulty performance for high SNR values in Fig 6.8, RMSE values of the improved method converge to the optimum Root and Spectral MUSIC methods estimations with correct array configuration. However, similar with the previous case, MUSIC and G-MUSIC RLA performances are worse than the proposed method, for all SNR and snapshot values.

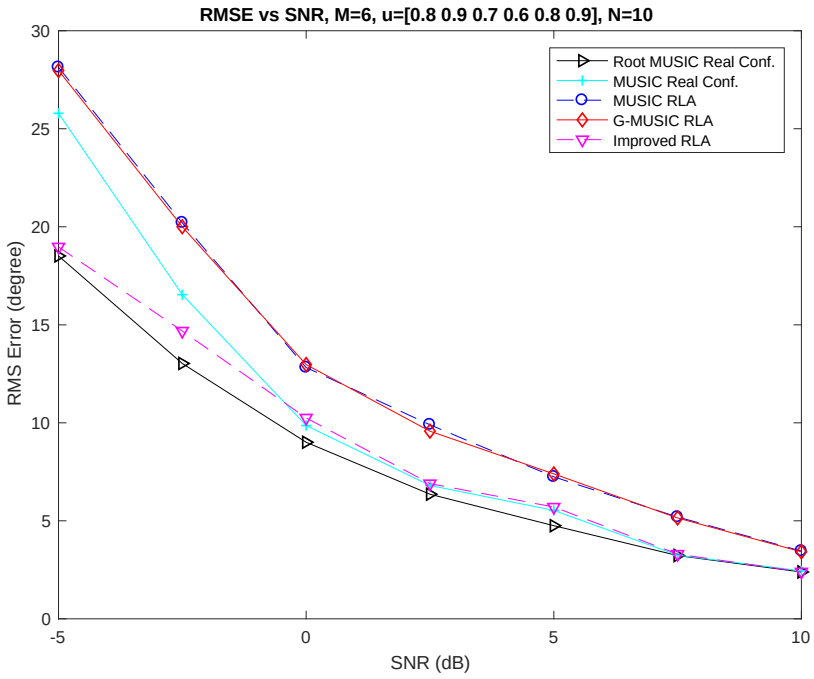

Figure 6.5. RMSE vs SNR, M=6, Each sensor Diff. Prob., N=10

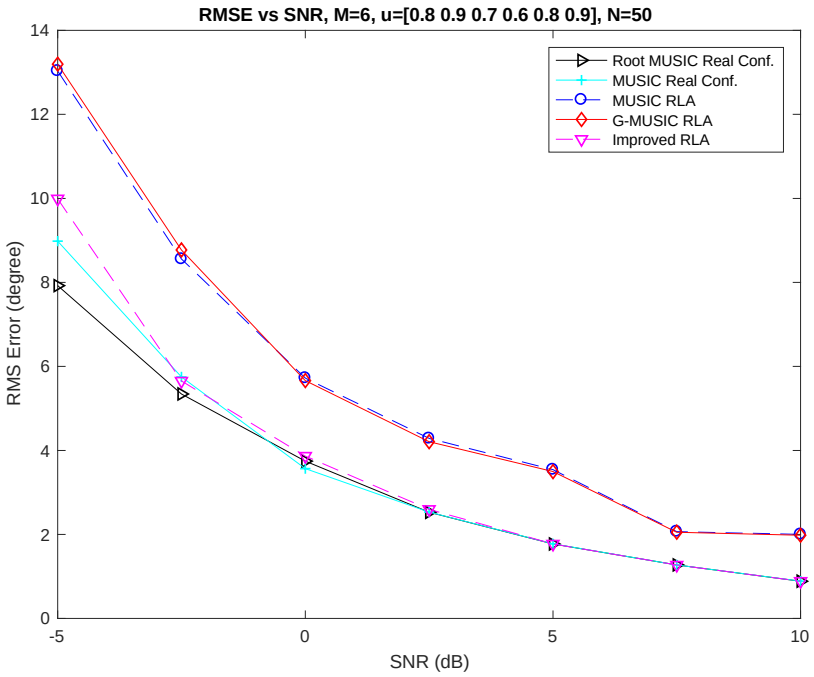

Figure 6.6. RMSE vs SNR, *M*=6, Each sensor Diff. Prob., N=50

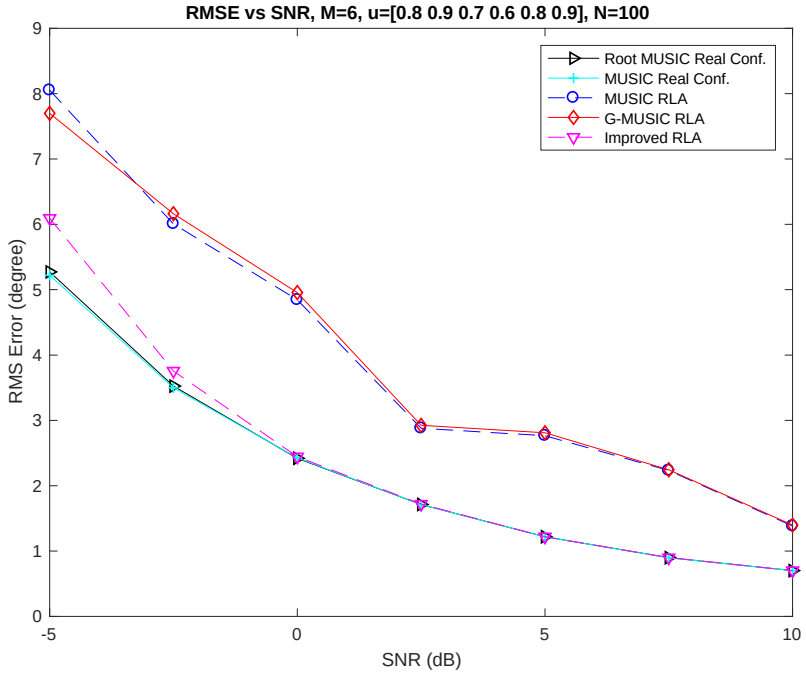

Figure 6.7. RMSE vs SNR, *M*=6, Each sensor Diff. Prob., N=100

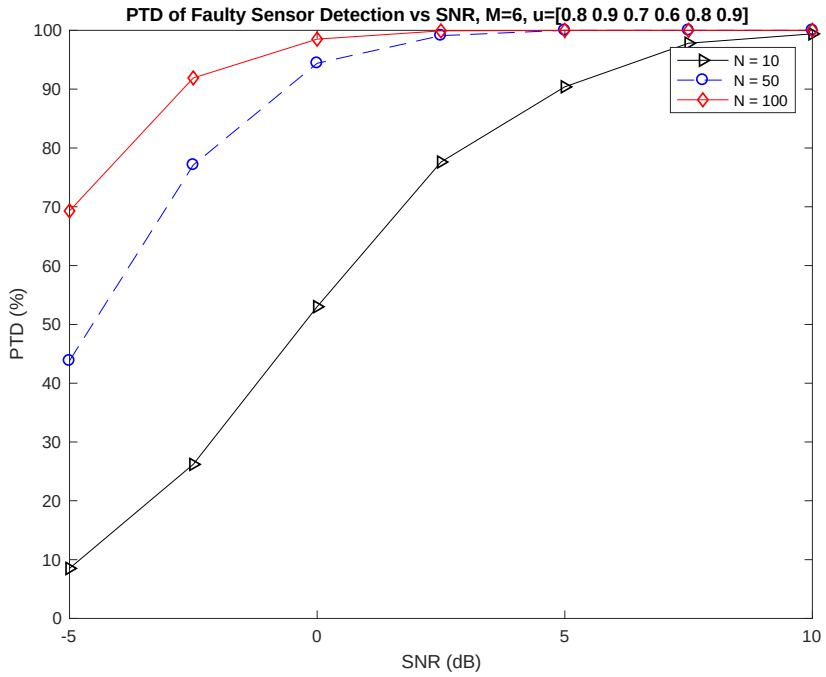

Figure 6.8. PTD of Faulty Sensor Detection vs SNR, M=6, Each sensor Diff. Prob.

6.2. Multiple Source Case

In multiple source scenario, the AOA of the sources are assumed to be at 20º and 70º. Number of sensors in the array is M=8, and all sensors are operating with p_i=0.8 possibility. Element spacing between the sensors in the array is chosen as $d = \frac{\lambda}{2}$. Since two source exist, total RMSE is computed by taking the RMS of two DOA estimation RMSE values.

Table 6.3. Multiple Source Case, M=8, p=0.8

Parameters	*Values*
M (Sensor number)	8
p (Operating sensor possibility)	0.8

L (Source Number)	2
SNR (dB)	[-5,10]
SNR Resolution (dB)	5
# of Monte Carlo runs	1000
N (Snapshots)	10, 50, 100
Spectral MUSIC Search Angle Resolution (deg)	0.1
AOA of Source Angle	20°, 70°
Spectral MUSIC Search Angle	[0º, 90º]

The results of multiple source case are presented in Fig 6.10-6.13. For the multiple source case, proposed method RMSE performance is observed to be better than MUSIC and G-MUSIC RLA method performances. Similar with the previous simulation results, as SNR goes higher the performance of improved method reaches the Spectral and Root-MUSIC Real Configuration performances. Different from the single case results, MUSIC and G-MUSIC RLA RMSE performances are achieving real configuration results around 10dB SNR. This is due to, MUSIC and G-MUSIC use the whole array structure and as much as the number of sensors in the array increases their RMSE values are decreasing. Consequentially, the proposed method is applicable for both single and multiple source cases with better performance results than related studies for randomly missing data. Finally, faulty sensor detection accuracy for multiple source case is similar with the single source case.

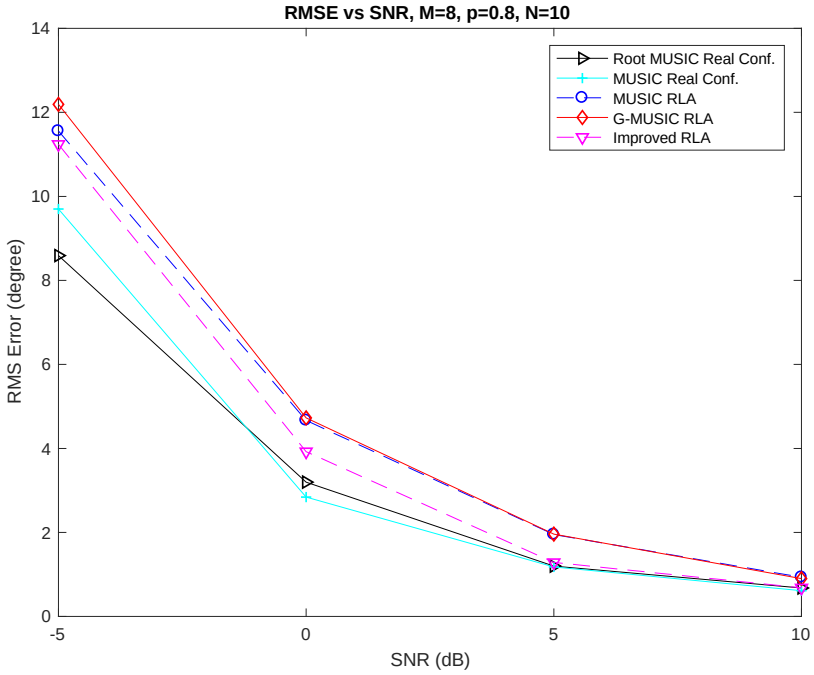

Figure 6.9. RMSE vs SNR, Multiple Source Case, *M*=8, p=0.8, N=10

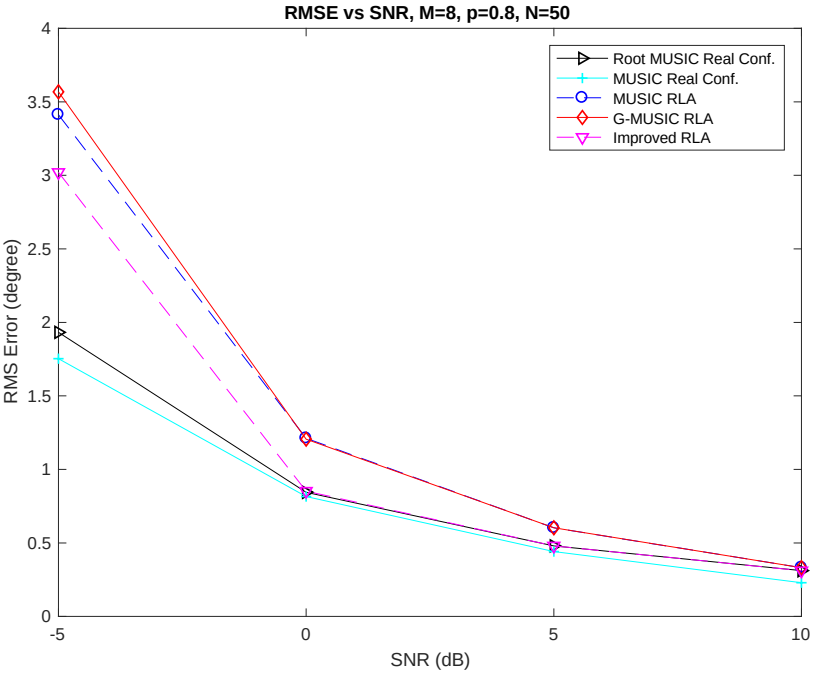

Figure 6.10. RMSE vs SNR, Multiple Source Case, *M*=8, p=0.8, N=50

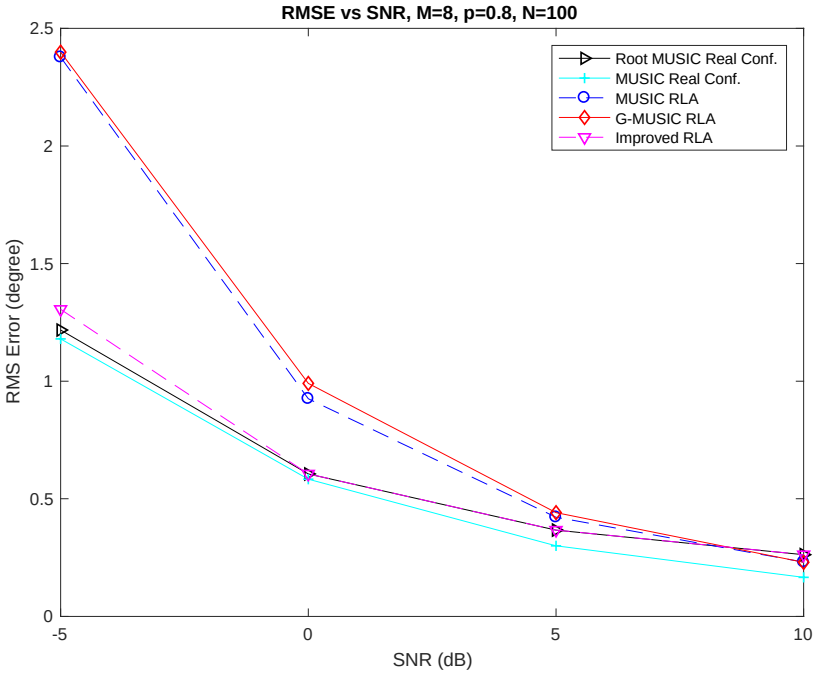

Figure 6.11. RMSE vs SNR, Multiple Source Case, M=8, p=0.8, N=100

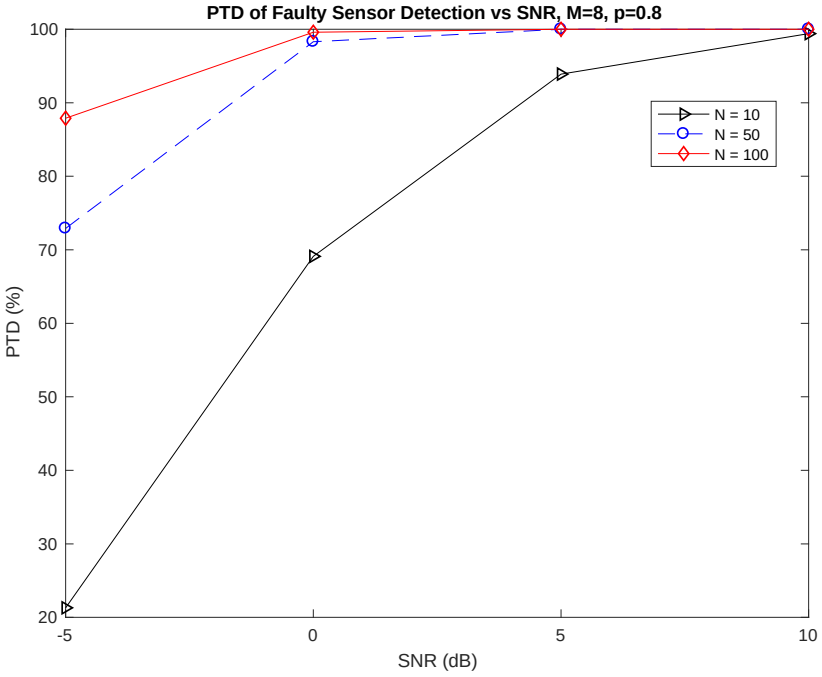

Figure 6.12. PTD of Faulty Sensor Detection vs SNR, Multiple Source Case, M=8, p=0.8

CHAPTER 7

CONCLUSIONS

In this thesis, two different problems are considered, namely the deterministic faulty sensors and random faulty sensors. In deterministic faulty sensors case, a special sensor array composed of MEMS microphones is investigated. MEMS microphones are produced on PCB's in such a way that two microphones share the same data channel. These microphones are configured to separate their output signal from the common data channel by using different edge of the clock signal, positive and negative cycles of clock. If one of the microphones is faulty, it cannot take the data channel and the data latched by the other microphone is still available for read. Hence when the microphone channels are read, two microphone signals became exact copies of each other. Hence, detection of faulty sensors in MEMS microphones without a physical intervention becomes a major problem. This thereby, leads us to propose a new method for determining faulty sensors by using a DOA known source. DOA known source enables us to compare the possible operating array configurations DOA performances by computing their PTD values, where the minimum absolute error among the possible configurations considered as true detection. According to the PTD values, the best matching one corresponds to the correct array configuration, resulting in detecting the faulty sensors. In the thesis work, detecting faulty sensors performances according to the DOA of known source is examined. In Chapter 4, the simulation results are presented with different scenarios, such as different SNR, known DOA source angles and sensor arrays to perform the abilities of the proposed method. As a result, the proposed method can find the faulty sensor or sensors accurately even in low SNR depending on the source position with respect to the array. Moreover, best angular region of the source with respect to the array is also presented in the results. Furthermore, the faulty sensor problem and detecting faulty sensors by using a DOA known source for MEMS microphones are reported for the first time in the literature.

In the second problem of the thesis, random faulty sensors are investigated. For the related problem, sensors in the array considered as stochastic live/faulty operation with an unknown probability for each sensor at any time. Random faulty sensors lead to randomly missing data with performance loss in DOA estimation applications. Related studies to the randomly missing data problem suggest a consistent DOA estimator by using the whole sensors in the array, without detecting the faulty ones. However, our motivation for randomly missing data problem is to detect the faulty sensors and achieve better DOA performance than the related studies. To achieve this goal, random sensor array features are examined and a new method is proposed. The results are presented in Chapter 6 for different scenarios, such as different SNR, operating possibilities, snapshots and sensor arrays, to perform the abilities of the proposed method. It is shown that the performance of the proposed algorithm is better than G-MUSIC algorithm's which G-MUSIC is a consistent DOA estimator for random linear array. Moreover, according to the results, at high SNR values performance of the proposed algorithm reaches to the performance of Spectral or Root-MUSIC using the correct operating sensors array configuration. This is due to faulty sensors are detected accurately at high SNR values. Additionally, it is shown that the proposed method is applicable for multiple source cases. Finally, the proposed method can be used for practical applications even for the low SNR cases.

Main disadvantage of the given random array method is the computational intensity comparing with other algorithms. The computational intensity is due to estimating each possible array configuration DOA. However, this disadvantage can be ignored by taking into consideration of improved DOA performance for random sensor arrays.

In our future work, faulty sensor problems could be further investigated. Deterministic approach could be improved by considering different types of faulty sensors and different array structures. In addition, detecting faulty sensors by using multiple known DOA source could be investigated. Future work for random array approach is utilizing different array geometries, although ULA geometry is used in the thesis work.

REFERENCES

[1] T. Engin Tuncer, Classical and Modern Direction-of-Arrival Estimation, Access Online via Elsevier, 2009

[2] I. Russo, P. Baldonero, A. Manna, D. Marcantoni and F. Trotta, High Resolution ESM/ELINT DOA estimation with super-heterodyne multi-octave antenna system, 2015 9th European Conference on Antennas and Propagation (EuCAP), Lisbon, 2015, pp. 1-5.

[3] P. S. T. Steen, G. F. Stott and F. Fallside, The application of feed-forward connectionist models to ESM bearing estimation using signal amplitude, IEE Colloquium on Signal Processing Techniques for Electronic Warfare, London, UK, 1992, pp. 4/1-4/6.

[4] G. F. Stott, DF Algorithms for ESM, In Military Microwaves'88, 1988

[5] O. A. Oumar, M. F. Siyau and T. P. Sattar, Comparison between MUSIC and ESPRIT direction of arrival estimation algorithms for wireless communication systems, The First International Conference on Future Generation Communication Technologies, London, 2012, pp. 99-103.

[6] Amidfa, K. & Tsoulos, G.V. & Nix, A. Performance evaluation of direction-of-arrival (DOA) estimation algorithms for mobile communication systems. Vehicular Technology Conference, 1988, IEEE 38th. 2. 1055 - 1059 vol.2.

[7] H. Wei and Y. Shi, Performance analysis and comparison of correlative interferometers for direction finding, IEEE 10th International Conference on Signal Processing Proceedings, Beijing, 2010, pp. 393-396.

[8] R. Schmidt, Multiple emitter location and signal parameter estimation, in IEEE Transactions on Antennas and Propagation, vol. 34, no. 3, pp. 276-280, March 1986.

[9] S. V. Schell, Performance analysis of the cyclic MUSIC method of direction estimation for cyclostationary signals, in IEEE Transactions on Signal Processing, vol. 42, no. 11, pp. 3043-3050, Nov. 1994.

[10] M. L. McCloud and L. L. Scharf, A new subspace identification algorithm for high-resolution DOA estimation, in IEEE Transactions on Antennas and Propagation, vol. 50, no. 10, pp. 1382-1390, Oct. 2002.

[11] N. Yuen and B. Friedlander, Asymptotic performance analysis of ESPRIT, higher order ESPRIT, and virtual ESPRIT algorithms, in IEEE Transactions on Signal Processing, vol. 44, no. 10, pp. 2537-2550, Oct. 1996.

[12] B. Ottersten, M. Viberg and T. Kailath, Performance analysis of the total least squares ESPRIT algorithm, in *IEEE Transactions on Signal Processing*, vol. 39, no. 5, pp. 1122-1135, May 1991.

[13] Zhang, Xin & Huang, Jingchang & Song, Enliang & Liu, Huawei & Li, Baoqing & Yuan, Xiaobing, Design of Small MEMS Microphone Array Systems for Direction Finding of Outdoors Moving Vehicles. Sensors, 2014.

[14] Kotus, Józef & Szwoch, Grzegorz, Calibration of acoustic vector sensor based on MEMS microphones for DOA estimation. Applied Acoustics. 141. 307-321, 2018.

[15] Infineon, IM69D130 High performance digital XENSIV MEMS microphone, Datasheet 2017.

[16] R. T. Suryaprakash and R. R. Nadakuditi, Consistency and MSE Performance of MUSIC-Based DOA of a Single Source in White Noise With Randomly Missing Data, in IEEE Transactions on Signal Processing, vol. 63, no. 18, pp. 4756-4770, 2015.

[17] R. T. Suryaprakash and R. R. Nadakuditi, "The performance of music-based DOA in white noise with missing data," *2012 IEEE Statistical Signal Processing Workshop (SSP)*, Ann Arbor, MI, 2012, pp. 800-803.

[18] SoDaRCAM. http://atarget.com.tr/eng/products/sound_cam.pdf

[19] S. U. Pillai and B. H. Kwon, Forward/backward spatial smoothing techniques for coherent signal identification, in IEEE Transactions on Acoustics, Speech, and Signal Processing, vol. 37, no. 1, pp. 8-15, Jan. 1989

[20] B. D. Rao and K. V. S. Hari, Performance analysis of Root-Music, in IEEE Transactions on Acoustics, Speech, and Signal Processing, vol. 37, no. 12, pp. 1939-1949, Dec. 1989.

[21] Carine El Kassis, Jose Picheral, Chafik Mokbel. Advantages of nonuniform arrays using Root-MUSIC. Signal Processing, Elsevier, 90 (2), pp.689-695, 2010.

[22] Harald Cramér, Mathematical Methods of Statistics (PMS-9), Volume 9, Princeton University press, 1999.

[23] B. D. Rao and K. V. S. Hari, Performance analysis of Root-Music, in IEEE Transactions on Acoustics, Speech, and Signal Processing, vol. 37, no. 12, pp. 1939-1949, Dec. 1989.

[24] Mestre, Xavier & Lagunas, Miguel, Modified Subspace Algorithms for DoA Estimation With Large Arrays. Signal Processing, IEEE Transactions on. 56. 598 – 614, 2008

[25] Vallet, P. & Loubaton, Philippe & Mestre, X., A statistical comparison between music and G-music. 2829-2833., 2015

[26] Mestre, Xavier, On the Asymptotic Behavior of the Sample Estimates of Eigenvalues and Eigenvectors of Covariance Matrices. Signal Processing, IEEE Transactions on. 56. 5353 – 5368, 2008.

[27] Zhou, Han-Fei & Huang, Lei & So, H.C. & Li, Jian, Performance analysis of G-MUSIC based DOA estimator with random linear array: A single source case. Signal Processing. 142, 2017.

[28] Arthur, David & Vassilvitskii, Sergei, K-Means++: The Advantages of Careful Seeding. Proc. of the Annu. ACM-SIAM Symp. on Discrete Algorithms. 8. 1027-1035, 2007.